



HAL
open science

Possible Atmospheric Diversity of Low Mass Exoplanets – Some Central Aspects

J.L. Grenfell, J. Leconte, F. Forget, M. Godolt, O. Carrión-González, L. Noack, F. Tian, H. Rauer, Fabrice Gaillard, E. Bolmont, et al.

► To cite this version:

J.L. Grenfell, J. Leconte, F. Forget, M. Godolt, O. Carrión-González, et al.. Possible Atmospheric Diversity of Low Mass Exoplanets – Some Central Aspects. *Space Science Reviews*, 2020, 216 (5), 10.1007/s11214-020-00716-4 . insu-02917578

HAL Id: insu-02917578

<https://insu.hal.science/insu-02917578>

Submitted on 5 Jan 2021

HAL is a multi-disciplinary open access archive for the deposit and dissemination of scientific research documents, whether they are published or not. The documents may come from teaching and research institutions in France or abroad, or from public or private research centers.

L'archive ouverte pluridisciplinaire **HAL**, est destinée au dépôt et à la diffusion de documents scientifiques de niveau recherche, publiés ou non, émanant des établissements d'enseignement et de recherche français ou étrangers, des laboratoires publics ou privés.

Possible Atmospheric Diversity of Low Mass Exoplanets – some Central Aspects

John Lee Grenfell¹, Jeremy Leconte², François Forget³, Mareike Godolt⁴, Óscar Carrión-González⁴, Lena Noack⁵,
Feng Tian⁶, Heike Rauer^{1,4,5}, Fabrice Gaillard⁷, Émeline Bolmont⁸, Benjamin Charnay⁹ and Martin Turbet⁸

(1) Institut für Planetenforschung (PF)
Deutsches Zentrum für Luft- und Raumfahrt (DLR)
Rutherfordstr. 2
12489 Berlin
Germany

(2) Laboratoire d'Astrophysique de Bordeaux (LAB)
Université Bordeaux
Centre National de la Recherche Scientifique (CNRS) B18N
Alle Geoffroy Saint-Hilaire
33615 Pessac
France

(3) Laboratoire de Météorologie Dynamique (LMD)
Institut Pierre Simon Laplace Université
4 Place Jussieu
75005 Paris
France

(4) Zentrum für Astronomie und Astrophysik (ZAA)
Technische Universität Berlin (TUB)
Hardenbergstr. 26
10623 Berlin
Germany

(5) Institut für Geologische Wissenschaften
Freie Universität Berlin (FUB)
Malteserstr. 74-100
12249 Berlin
Germany

(6) Macau University of Science and Technology
Taipa, Macau

(7) CNRS Orléans Campus
Institut des Sciences de la Terre d'Orléans (ISTO)
1A Rue de la Ferrollerie Campus Géosciences
45100 Orléans
France

(8) Observatoire Astronomique de l'Université de Genève
Observatoire de Genève
Chemin de Pégase, 51
1290 Versoix
Switzerland

(9) Observatoire de Paris (OP)
Site de Meudon – 5
Place Jules Janssen
F-92195 Meudon cedex
Paris

66 *Abstract: exoplanetary science continues to excite and surprise with its rich diversity. We discuss here some key*
67 *aspects potentially influencing the range of exoplanetary terrestrial-type atmospheres which could exist in nature.*
68 *We are motivated by newly emerging observations, refined approaches to address data degeneracies, improved*
69 *theories for key processes affecting atmospheric evolution and a new generation of atmospheric models which*
70 *couple physical processes from the deep interior through to the exosphere and consider the planetary-star system*
71 *as a whole. Using the Solar System as our guide we first summarize the main processes which sculpt atmospheric*
72 *evolution then discuss their potential interactions in the context of exoplanetary environments. We summarize*
73 *key uncertainties and consider a diverse range of atmospheric compositions discussing their potential occurrence*
74 *in an exoplanetary context.*

75
76
77
78
79
80
81
82
83
84
85
86
87
88
89
90
91
92
93
94
95
96
97
98
99
100
101
102
103
104
105
106
107
108
109
110
111
112
113
114
115
116
117
118
119
120
121
122
123
124
125
126
127
128
129
130

Key words: *exoplanetary, atmospheres, diversity, review*

131 1. Introduction

132 Exoplanetary science at the dawn of the 2020s lies at a fascinating juncture at which the basic
 133 atmospheric properties of potentially rocky worlds lying in the habitable zone are already beginning to be
 134 constrained (see e.g. de Wit et al., 2018 which focused on TRAPPIST-1 planets in the Habitable Zone). Earlier
 135 works such as Forget and Lecote (2014) have discussed the potential diversity of exoplanetary atmospheres.
 136 Some new aspects were recently summarized by Jontof-Hutter (2019) and Madhusudhan (2019). Tinetti et al.,
 137 (2018) summarized a chemical survey of exoplanets with the Atmospheric Remote-Sensing Infrared Exoplanet
 138 Large-Survey (ARIEL) mission. In the present review we highlight some recent aspects relevant for potential
 139 exoplanetary diversity for terrestrial-type exoplanets up to ~ 10 Earth masses. It is beyond the scope of our work
 140 however to review all aspects of this rapidly developing field.

141 There are numerous developments which motivate our review. First, improved mass-radius data for
 142 cooler mini gas planets and super-Earths (see e.g. Fulton et al., 2017; Fulton and Petigura, 2018; Weiss and Marcy,
 143 2014) are confirming that exoplanetary mass can vary over several orders of magnitude for a given radius
 144 whereas radius can vary by up to a factor of ~ 4 for a given mass. Small planets are being found which lie above
 145 the pure water composition line in the mass radius diagram - which suggests they have atmospheres. Emerging
 146 measurements are providing initial observational constraints for the atmospheres of hot Super Earths. Such new
 147 data is providing first hints of atmospheric diversity and is driving emerging strategies for addressing the
 148 challenging degeneracies involved as discussed in e.g. Dorn et al. (2017) and Dorn and Heng (2018). Second,
 149 progress in detection methods has been made for several atmospheric species. These include theoretical studies
 150 involving spectroscopy of collisional pairs as a potential proxy for O_2 -rich (Schwieterman et al., 2016) and N_2 -rich
 151 atmospheres (Schwieterman et al., 2015; new proposed pathways for abiotically produced CO and O_2 (Wang et
 152 al., 2016); observational constraints for escaping helium (Spake et al., 2018) on a giant exoplanet as well as new
 153 predictions for the mass and characteristic timescales of thin silicate atmospheres on magma ocean worlds (see
 154 e.g. Kite et al., 2016). Third, progress has been made regarding key processes such as escape (Owen, 2019)
 155 (including early water loss, see Tian et al., 2018) and outgassing (e.g. Gaillard and Scaillet, 2014) over evolutionary
 156 timescales. These are being complimented by a growing database of observationally constrained escape rates
 157 from exoplanetary atmospheres. Fourth, there have been numerous studies on newly-discovered planetary
 158 systems such as TRAPPIST-1 (Gillon et al., 2017) and Proxima Centauri-b (Anglada-Escudé et al., 2016). With the
 159 above in mind, we focus in our review on a specific selection of potential exoplanetary atmospheric compositions
 160 e.g. based on hydrogen, oxygen, water, silicate, halogen, hydrocarbon, sulfur etc. species and discuss their
 161 potential properties and feasibility.

162 Section 2 introduces key processes and their uncertainties. Section 3 gives a brief overview of
 163 atmospheric diversity in the Solar System. Section 4 discusses some key phenomena affecting exoplanetary
 164 diversity. Section 5 discusses individual exoplanetary atmospheres. Section 6 presents the conclusions.
 165

166 2. Key Processes

167 We provide here an initial brief summary of some key processes affecting atmospheric diversity. These
 168 include (1) *gas accretion* of growing protoplanets in the disk. Key uncertainties here are the timescales for
 169 protoplanetary growth and gas evaporation (Lammer et al., 2018); the role of planetary migration and the
 170 dynamical mechanism(s) for volatile delivery (Jacobson and Morbidelli, 2014); (2) Primary (catastrophic)
 171 *outgassing* at the end of the magma ocean phase and secondary (volcanic) outgassing. Uncertainties here are
 172 related to material properties, convection and composition of the interior; (3) *Delivery* via impacts. Uncertainties
 173 involve the effect of impactor properties (mass, composition, radius) over time (De Niem et al., 2012); (4)
 174 *Atmospheric escape* which can be broadly split into *thermal* (Jeans, hydrodynamic) and *non-thermal* (sputtering,
 175 pickup etc.) escape (see e.g. Tian, 2015a). A key uncertainty here is the evolution of stellar XUV (from 10-91.2nm)
 176 which drives atmospheric escape (see e.g. Johnstone et al., 2015; Tian, 2015a). Related processes important for
 177 atmospheric development include biogeochemical cycling, weathering, biomass emissions, climate and
 178 photochemistry.
 179

180 3. Lessons from the Solar System for Exoplanetary Science

181 The modern and early Solar System offer valuable lessons for understanding atmospheric diversity.
 182 Figure 1 provides a general overview:

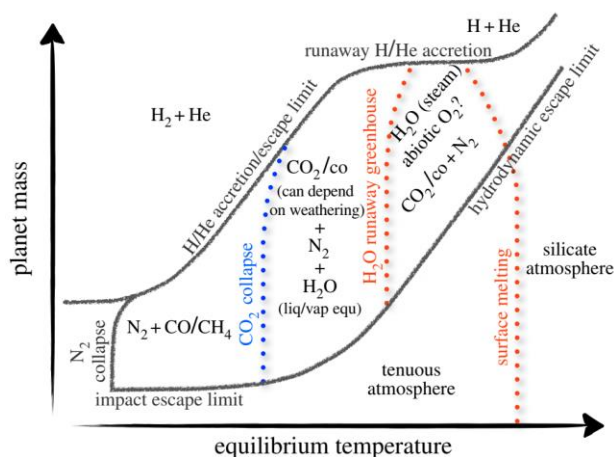


Figure 1: Schematic of atmospheric diversity taken from Forget and Leconte (2014).

We now briefly discuss Solar System atmospheres with reference to the regions in Figure 1.

3.1 Tenuous atmospheres – are defined here as objects with surfaces pressure less than a few tens of microbars. They are favored for smaller bodies with weak, gravitational fields or/and strong incoming insolation. Examples are modern Mercury, the Moon, the Galilean Satellites, Pluto and Triton. Table 1 (Grenfell, 2009 and references therein unless otherwise stated) provides a brief overview:

Body	Species	Species Amount	Total Surface Pressure	Reference
Mercury	Helium	$\sim 3 \cdot 10^{11}$ molecules cm^{-2}	$< 10^6$ molecules cm^{-3}	Grenfell (2009) and references therein
	Calcium	$\sim 1.3 \cdot 10^{11}$ molecules cm^{-2}		
	Sodium	$\sim (1-2) \cdot 10^{11}$ molecules cm^{-2}		
	Argon	$\sim (0.5-1.2) \cdot 10^{9\text{S}}$ molecules cm^{-2}		
Moon	Helium	$\sim (2-40) \cdot 10^3$ molecules cm^{-3} (P_0)	$8 \cdot 10^4$ molecules cm^{-3}	Stern et al. (1994)
	Argon	$4 \cdot 10^4$ molecules cm^{-3} (P_0)		
Io	Sulfur dioxide	$10^{-12}-10^{-7\#}$ surface in bar (P_0)		
Europa	Atomic oxygen	10^{-11} bar (P_0)		Hall et al. (1995)
Ganymede	Molecular oxygen	$\sim (1-10) \cdot 10^{14}$ (P_0)	$< 2 \cdot 10^{-11}$ (bar)	Hall et al. (1998)
Callisto	Carbon dioxide	$7.5 \cdot 10^{-12}$ bar (P_0)		Carlson (1999)
Pluto	Molecular nitrogen	0.98 vmr (P_0)	$\sim 1 \cdot 10^{-5}$ (bar)	Grenfell (2009); Wong et al. (2017)
	Methane	$10^{12}-10^{13}$ molecules cm^{-2}		
Triton	Molecular nitrogen		$1.9 \cdot 10^{-5}$ (bar)	Gladstone et al. (2016) ^{oo}

Table 1: Overview of tenuous atmospheres in the Solar system. P_0 denotes surface value. ^SUncertain, weak outgassing source. ^{SS}Stern et al. (1994), their Table 6. [#]Variable due to freeze-out at high-latitudes, Yung and DeMore (1999). ^{oo}N₂-dominated.

The extremely thin atmospheres (“collisionless exospheres”) can be strongly influenced by sputtering from the solar wind (a source of helium e.g. for Mercury and the Moon, Table 1) and by surface mineral properties. The recent *MERcury Surface, Space ENVIRONMENT, GEOchemistry and RANGING (MESSENGER)* mission revolutionized knowledge of Mercury’s alkali metal exosphere (see e.g. Merkel et al., 2017) and near-atmosphere gas-phase ion concentrations (Raines et al., 2014) useful for interpreting atmospheric evolution. Atmospheres of the Galilean moons could be influenced by sputtering onto ice surfaces which splits water and releases oxygen-containing compounds (Table 1).

208 3.1.1 Exoplanetary context

209 Tenuous atmospheres have been proposed for ultra-short period (USP) (periods of <1day) hot Super-
 210 Earths (SEs) such as CoRot-7b (Léger et al., 2009), Kepler-10b (Batalha et al., 2011), 55 Cancri e (Demory et al.,
 211 2011) and HD80653 (Frustagli et al., 2020) plus several others (see e.g. Guenther and Kislyakova, 2020 and
 212 references therein). These highly-irradiated worlds could represent the stripped cores of smaller hot gas planets
 213 but possibly retaining thin atmospheres e.g. derived from refractory material such as silicate (see discussion in
 214 Lopez and Rice, 2018) whereas larger, less irradiated SEs could retain their volatile envelopes. Planetary
 215 population diagrams (e.g. Fulton et al., 2017; Lundkvist et al., 2016) suggest a radius minimum separating rocky
 216 SEs from mini gas planets which is a focus of numerous modeling studies (e.g. Mordasini, 2020). A central issue
 217 is whether hot SEs formed mostly in-situ or underwent inward migration which likely depends upon the central
 218 properties and timescales of the protoplanetary disk (see e.g. Raymond and Cossou, 2014; Martin and Livio,
 219 2016). Direct observations of the proposed tenuous atmospheres of hot SEs is rather lacking although proxy data
 220 for atmospheric mass and composition is emerging.

221 Regarding Corot-7b earlier model studies (e.g. Schaefer and Fegley, 2009) suggested silicate
 222 atmospheres with strong sodium and calcium absorption lines analogous to Mercury and Io. Kurokawa and
 223 Kaltenecker (2013) suggested that XUV-driven photoevaporative loss could remove one Jupiter mass of gaseous
 224 envelope on Corot-7b (and Kepler 10b) within ~1Gyr. Guenther et al. (2011) placed upper limits for alkali metals
 225 based on atmospheric spectral features for CoRot-7b. Samuel et al. (2014) implied that obtaining a few transits
 226 with the James Webb Space Telescope (JWST) could extend such analyses by constraining atmospheric mass and
 227 composition of CoRot-7b. Regarding Kepler-10b, Rouan et al. (2011) suggested the observed phase curves were
 228 best fitted by a rather high bond albedo of ~0.5 with a tenuous ($p_0 < 2\text{mb}$) silicate atmosphere (see also Herbort
 229 et al. (2020) who discuss theoretical atmospheres which can form above a (partially) melted crust). By
 230 comparison Esteves et al., (2015) derived mostly lower albedos of <0.25 a sample of 14 close-orbiting Kepler
 231 mission planets

232 Regarding 55 Cancri e, phase curve data (Tsiaris et al., 2016) based on the Hubble Space Telescope (HST)
 233 Wide Field Camera (WFC3) suggested a hydrogen-helium dominated atmosphere with the surface pressure
 234 posterior peaking at 100mb (although this quantity was only loosely constrained) and a possible detection of
 235 hydrogen cyanide (HCN). High resolution transit spectroscopy (Ridden-Harper et al., 2016) suggested a modest
 236 (3σ) sodium detection which would be consistent with an exosphere extending to ~five planetary radii. Spitzer
 237 thermal flux observations (Demory et al., 2016^b) suggested a strong (~1300K) gradient between the dayside and
 238 the nightside of 55 Cancri e which implies either a thin atmosphere or weak transport from day to night. Assuming
 239 partial vaporization and surface exchange from molten magma pools, Kite et al. (2016) suggested a tenuous
 240 atmosphere with a surface pressure of ~10Pa (~ 10^{-5} bar) on 55 Cancri e. Angelo and Hu (2017) however suggested
 241 a rather thick atmosphere with a surface pressure of ~1.4 bar based on a model fitted to time series of Spitzer IR
 242 photometry. Hammond and Pierrehumbert (2017) applied a General Circulation model to 55 Cancri e which
 243 suggested that a light (90:10, H₂:N₂) atmosphere with several bars surface pressure could best fit the phase curve
 244 data. Lightcurve observations including revised stellar activity (Bourrier et al., 2018) however did not support
 245 such a lightweight atmosphere. Miguel (2019) and Zilinskas et al. (2020) subsequently modeled the detectability
 246 of atmospheric spectral features by JWST assuming heavy, nitrogen-dominated atmospheres on 55 Cancri e
 247 varying [C/O] from 0.01 to 200. Results suggested e.g. that HCN should be clearly detectable for high C/O
 248 scenarios. Variability in 55 Cancri e lightcurves (e.g. Demory et al., 2016^a; Tambura et al., 2018 and Sulis et al.,
 249 2019) could arise due to e.g. stellar variability or due to a possible dust torus. The latter work suggested upper
 250 constraints on the optical albedo (<0.47 at 2-sigma) for 55 Cancri e based on the non-detection of secondary
 251 eclipses in visible light with the Microvariability and Oscillation of Stars (MOST) satellite. Folsom et al. (2020)
 252 modelled the stellar wind based on Zeeman Doppler Imaging and concluded that 55 Cancri e orbits inside the
 253 Alfvén surface which suggests that planet-star interactions could occur. Dorn et al. (2019) applied an interior
 254 model using a Bayesian approach which suggested that 55 Cancri e could have a mantle enriched in calcium and
 255 aluminium and may even lack a planetary core which would have poorly-known consequences for atmospheric
 256 evolution via outgassing. Modirrousta-Galian et al. (2020) suggested strong tidal forces could trap light
 257 atmospheres on the nightside where they could survive stellar driven escape.

258 In summary, a range of atmospheric masses and compositions have been suggested based on
 259 observations of Cancri 55e over the last decade. This could arise because such measurements approach the
 260 capability limits of modern instrumentation, or possibly due to intrinsic variability in the atmosphere via e.g.
 261 volcanism, or due to external variability via e.g. stellar luminosity or dust. Follow-up observations with JWST
 262 should help address these issues.

263 Tenuous exo-atmospheres are favoured targets in the sense that they could be sampled *over their entire*
 264 *vertical extent* by exoplanetary transmission spectroscopy. For thicker atmospheres one typically samples only
 265 the upper regions since the underlying layers (pressures in the range of about (10 -100) millibars depending on

266 wavelength and composition) become optically-thick or the light is refracted away from the observer (García
 267 Muñoz et al., 2012; Bétrémieux and Kaltenegger, 2014). Tenuous atmospheres will therefore more likely offer
 268 atmospheric windows sampling down to the surface potentially revealing surface mineralogy (although
 269 identifying spectral signals of exoplanetary surfaces is observationally very challenging, see Hu et al., 2012;
 270 Madden and Kaltenegger, 2020) which via sputtering could influence the main atmospheric constituent - as on
 271 Mercury (Table 1). Also, such worlds could have extensive tails of e.g. sodium extending out to several planetary
 272 radii - as on Mercury (Potter and Killen 2008) and on the Moon (Matta et al., 2009). Such “cometary-like tails”
 273 have also been found for Hot Neptunes such as GJ436b in the form of escaping hydrogen (Kulow et al., 2014;
 274 Ehrenreich et al., 2015) and for super-Mercuries in the form of dust (Budaj, 2013). Upper atmosphere detections
 275 of atomic species (although currently most such detections have so far been achieved mostly for hot Jupiters,
 276 see Madhusudhan et al., 2016 and references therein) could be early probes of atmospheric composition.

277 Close-orbiting planets are on the one hand favored targets due to short orbital periods which suggest a
 278 high number of transit events over a given period. On the other hand, tenuous exo-atmospheres are generally
 279 favored by smaller bodies with smaller transit depths which vary proportional to the factor (r_p^2/r^2). Also, low
 280 mass atmospheres in general could lead to weak planetary absorption features. Korabev et al. (this issue, chapter
 281 14) and Tinetti et al. (this issue, chapter 16) discuss future observations of exoplanetary atmospheres from space.

282
 283 **3.1.2 Lessons for Exoplanetary Diversity** – for Mercury-like worlds, observations from the Solar System suggest
 284 atmospheres could consist of (1) a helium component depending on e.g. planetary protection and the impinging
 285 stellar wind, (2) a gas-phase alkali metal component depending on e.g. the availability of alkali minerals and
 286 surface mineralogy and (3) a smaller (about x100 less) amount of outgassed noble gases. Regarding point (1),
 287 Vidotto and Bourrier (2017) (their Table 1) summarize estimates of stellar mass loss rates and atmospheric extent
 288 for different stellar classes. Boro Sakia et al. (2020) suggest that current model estimates of stellar wind
 289 properties such as mass and momentum loss rates could vary by a factor (2-10). Regarding point (2), the
 290 theoretical study by Hu et al. (2012) suggested that JWST could possibly identify e.g. surface silicate IR bands for
 291 some nearby targets although this will be very challenging.

292

293 **3.2 Silicate Atmospheres**

294 The inner rocky planets and the Moon experienced an early period of intense bombardment lasting for
 295 a few hundred million years after formation. This led to local and global magma ocean (MO) events. Zahnle et al.
 296 (2010) suggested early hot rock (silicate) atmospheres having characteristic removal timescales of up to ~1000
 297 years with silicate rainout proceeding via the condensation rock sequence (e.g. corundum, forsterite, wüstite
 298 etc.). The order of condensation is uncertain depending upon the reducing nature of the MO-atmosphere system
 299 which is likely sensitive to the rate of iron rainout into the core as it formed. Pahlevan et al. (2011) discussed hot
 300 rock rainout on early Earth calculated with a two-phase thermodynamical model having magnesium rich droplets
 301 in an iron rich vapor. Fegley and Schaefer (2012) reviewed studies of Earth’s silicate vapor atmosphere including
 302 rainout, (silicate) snow formation and in-situ photochemical reactions. Somewhat lacking in the literature are
 303 calculations of silicate atmosphere rainout using modern, time-dependent microphysical models. Direct spectral
 304 observations of silicate atmospheres on e.g. hot rocky SEs are very challenging but could be achieved with JWST
 305 (see also discussion in section 5.1.)

306

307 **3.3 Steam Atmospheres**

308 Atmospheres dominated by water vapor represent a critical phase for the early development of
 309 terrestrial planets. The timing and interplay between key processes such as escape and outgassing during the
 310 steam atmosphere phase can strongly influence the onset and duration of the planet’s subsequent habitability.
 311 The nature and magnitude of outgassing at the end of the MO phase is related to the progressive exclusion of
 312 volatiles from the minerals driven by bottom-up solidification and depends on cooling rates and convection
 313 turnover timescales (see e.g. Maurice et al., 2017; Boukaré et al., 2018). Crustal formation occurred on Earth
 314 between (10^4 - 10^7) years after the final global MO phase began (see e.g. Lebrun et al., 2012; Nikolaou et al., 2019).
 315 The range of uncertainty arises mainly due to poorly-constrained material properties of the mantle and
 316 uncertainties in atmosphere-interior coupling.

317 Regarding Venus-Earth-Mars (VEM) Lammer et al. (2018) and references therein (their Table 2)
 318 suggested catastrophic outgassing of (450, 200, 50) bars of water on VEM respectively. Lebrun et al. (2013)
 319 estimated that the first global oceans condensed (~0.1, 1.5, 10) Myr thereafter on VEM respectively. Way et al.
 320 (2016) suggested early Venus could be habitable up to $t=715$ Myr assuming one tenth of an Earth ocean based
 321 on their 3D model study. Lammer et al. (2018) however suggested that on Venus the steam atmosphere may
 322 never have condensed and the water could have been possibly lost via early escape. On Earth, numerous studies
 323 (e.g. Elkins Tanton et al., 2008; Elkins-Tanton et al., 2012; Hamano et al., 2013; Lebrun et al., 2013; Massol et al.,

2016; Salvador et al., 2017) investigated how the early thick steam atmosphere formed, cooled, condensed and ultimately formed the oceans. Model studies (e.g. Katyal et al., 2019) investigated cooling of Early Earth's steam atmosphere due to outgoing longwave (LW) radiation at different stages of the MO.. Earth proxy data (ancient zircons) support early oceans 4.3 to 4.4 Gyr ago (Mojzsis et al., 2001). Direct spectral observations of giant steam atmospheres in an exoplanet context are currently lacking.

329

3.4 Carbon Dioxide (CO₂) - Nitrogen (N₂) - Oxygen (O₂) Atmospheres

After the onset of Earth's oceanic and continental formation, carbon dioxide was increasingly subject to atmospheric removal via washout and weathering. The role of atmospheric escape weakened as the early stellar EUV output decreased (e.g. Ribas et al., 2005). Other long-term processes also began to play a role for subsequent atmospheric evolution. These involved wide-ranging and sometimes subtle feedbacks within the interior-hydrosphere-lithosphere-biosphere-atmosphere system (see e.g. Spohn, 2014). Processes such as secondary outgassing, weathering (continent formation), climate, photochemistry, feedback cycles and eventually biology and biogeochemical cycles of carbon, nitrogen and oxygen (discussed below) start to influence atmospheric evolution. Charnay et al., (this issue, chapter 3) review climate evolution on the Early Earth and the faint young sun problem.

340

3.4.1 Volatile Inventory of Earth's chondritic building blocks

To gain insight into the volatile budget of the basic building blocks of our planet, Tables 2 and 3 show the gas compositions at p=100 bar which are in equilibrium with the metal chondrites (Table 2) and the carbonaceous chondrites (Table 3) at 500K, 1000K and 2000K. Data is from Zahnle et al. (2010) their Figures 2 and 3 which are based on Schaefer and Fegley (2010):

346

Species	%Molar 500K	%Molar 1000K	%Molar 2000K
NH ₃	1.2	<1%	<1%
N ₂	<1%	<1%	<1%
H ₂ S	<1%	<1%	1.3
CO ₂	<1%	<1%	2.4
H ₂ O	<1%	6.3	18.6
CO	<1%	<1%	25.7
H ₂	<1%	25.1	47.9
CH ₄	94.4	64.6	<1%

347

Table 2: Gas compositions (%molar) at 100 bar which are in equilibrium with the metal chondrites (Schaefer and Fegley, 2010).

348

349

350

Species	%Molar 500K	%Molar 1000K	%Molar 2000K
NH ₃	<1%	<1%	<1%
N ₂	<1%	<1%	<1%
H ₂ S	<1%	<1%	4.2
CO ₂	66.1	21.9	15.1
H ₂ O	28.2	66.1	63.1
CO	<1%	1.4	<1%
H ₂	<1%	6.0	6.6
CH ₄	5.9	<1%	<1%
SO ₂	<1%	<1%	2.0

351

352

353

Table 3: As for Table 2 but for the carbonaceous chondrites.

Table 2 (iron chondrites) suggests the chemical equilibrium favors volatile speciation into methane and ammonia at lower temperatures, shifting to hydrogen, carbon monoxide and water at higher temperatures. Table 3 (carbonaceous chondrites) suggests that chemical equilibrium favors mainly carbon dioxide with some water at lower temperatures, shifting to mainly water with some carbon dioxide together with sulfur compounds

356

357

358 and hydrogen at higher temperatures. Fegley and Schaefer (2012) discuss theories for constraining the relative
 359 amounts of chondritic material making up the bulk Earth.

360

361 **3.4.2 Venus Earth Mars**

362 Numerous texts have discussed the present-day (e.g. Yung and DeMore, 1999) and evolutionary
 363 compositional development (e.g. Lammer et al., 2018) of CO₂-N₂-O₂ atmospheres on Venus, Earth and Mars (see
 364 also Lammer et al., 2020). Regarding Venus e.g. Lammer et al. (2018); Hamano et al., (2013) and Lebrun et al.,
 365 (2013) suggested that strong insolation compared to the Earth may have lengthened the steam atmosphere
 366 phase for long enough (~100 Myr) such that efficient hydrodynamic escape could have effectively dried out the
 367 planet. In this scenario, the thick, hot, modern CO₂ atmosphere on modern Venus results directly from outgassing
 368 at the end of the MO and *not* via the more frequently discussed runaway moist greenhouse effect. Regarding N₂,
 369 nitrogen isotope data (Marty, 2012) favors a carbonaceous chondrite origin. Some nitrogen in the form of NH₃
 370 (Lammer et al., 2018 and references therein) could have existed near the Venusian surface especially if the early
 371 atmosphere was shielded from UV.

372 Regarding Earth, weaker insolation than Venus and long-term plate tectonics maintained surface oceans
 373 with stabilizing climate feedbacks involving atmospheric CO₂ such as the carbonate-silicate cycle (Walker et al.,
 374 1981) (Charnay et al., this issue) discuss climate on Early Earth and the faint young Sun problem). The build-up
 375 of N₂-O₂ dominated atmospheres are favored by the presence of life (Lammer et al., 2018).

376 Regarding Mars, escape mainly drives atmospheric evolution. Odert et al. (2018) assumed outgassing of
 377 (CO₂=11bar) and (H₂O=85bar) at the end of the MO period and then calculated complete atmospheric loss via
 378 escape after 18 Myr (25 Myr) assuming a moderately (slowly) rotating early Sun. Supporting this, xenon data
 379 from ancient Martian meteorites suggest that early Mars lost most of its initial atmosphere (Cassata, 2017).
 380 Observations of modern Mars by the Mars Atmosphere and Volatile Evolution (MAVEN) spacecraft (Jakosky et
 381 al., 2018) suggested integrated loss rates (assuming Solar evolution) on Mars of 0.8 bar CO₂ and a 23m water
 382 ocean layer. Kite et al. (2019) review constraints in the evolution of atmospheric pressure and liquid water on
 383 early Mars based on geological data. Warren et al. (2019) suggested a continuous surface pressure upper limit
 384 of 1.9 bar at 4 Gyr on Mars based on an analysis of small craters. High Martian ¹⁵N compared to the other rocky
 385 planets suggests that Mars lost a significant amount of its early nitrogen inventory (Lammer et al., 2018).
 386 Regarding outgassing, the reduced Martian interior could favor enhanced outgassing of e.g. H₂ and CO compared
 387 with Earth (Ramirez et al., 2014). This could lead to an interior-atmosphere negative feedback whereby
 388 outgassing of reduced species on Mars leads to enhanced atmospheric loss of the reductant H which drives
 389 oxidation of the atmosphere and hence (via e.g. deposition) ultimately favors mantle oxidation over time. Catling
 390 et al. (2003) discussed similar mechanisms operating on Early Earth.

391

392 **3.4.3 Isotopic fractionation**

393 Several of the key process mentioned above e.g. escape, delivery and interior processes, result in
 394 isotopic fractionation. Numerous advances leading to reduced data precision for isotopic fractionation ratios
 395 have occurred in recent years. For example, Hin et al. (2017) suggested that accretional vaporization played an
 396 important role in the volatile budget of terrestrial planet formation based on improved isotopic magnesium
 397 ratios. New ruthenium isotope data (Fischer-Gödde and Kleine, 2017) suggested surprisingly that the late veneer
 398 featured an *inner* solar system origin and was likely not the primary source of volatiles on Earth. Improved noble
 399 gas and nitrogen isotope data has advanced knowledge of early escape, especially on Mars (Cassata, 2017; Furi
 400 and Marty, 2015) whereby observed neon and argon isotope ratios (Odert et al., 2018) support a slow to
 401 moderately rotating (rather than a quickly rotating) early Sun.

402

403 **3.4.4 Exoplanetary Context**

404 Inspecting volatile inventories of terrestrial planet building blocks (Tables 2 and 3) based on chondrites
 405 from the Solar System gives a general indication of the potential range of atmospheric species in an exoplanetary
 406 context where such observations are not available. Hints on exoplanetary mineral compositions can be gained
 407 from e.g. stellar metallicity measurements coupled with interior structure plus atmospheric escape modeling
 408 (Dorn and Heng, 2018). Planet formation and interior structure models (Alibert and Venturini, 2019) also provide
 409 some insight. Initial observations of infalling material from circumstellar debris onto white dwarfs as reviewed in
 410 Farihi (2016) have been performed. Results suggest exomineral compositions which are not dissimilar to those
 411 of the Solar System. Adibekyan et al. (2015) investigated observed [Mg/Si] ratios of [F,G,K] stars using HARPS.
 412 Their results suggested an evolution in this ratio through the Galaxy and that smaller mass stars have higher
 413 ratios. We now discuss briefly the key processes affecting atmospheric diversity of terrestrial exoplanets.

414 Regarding *escape*, progress is somewhat hindered by a lack of various parameters such as stellar EUV
 415 observations, stellar wind properties and planetary exospheric temperatures which can all influence atmospheric

416 escape. Improved estimates of such parameters e.g. improved stellar EUV by semi-empirical modeling (Fontenla
 417 et al., 2016) is useful in this regard. Section 4.3 discusses (extreme) escape processes in more detail. Regarding
 418 *outgassing*, numerous factors could be relevant which we will briefly discuss in approximate order of observing
 419 difficulty. The bulk planetary density can be estimated already today for some SEs by measuring planetary radius
 420 from the transit depth together with planetary mass from the radial velocity method. The planet's mass
 421 distribution throughout the interior can be in principle constrained by determining the love number although
 422 observations are presently limited to large, close-in exoplanets (e.g. Hellard et al., 2020). The core mantle ratio
 423 and interior composition can be constrained from Bayesian analyses (Dorn et al., 2015) and machine-learning
 424 (Baumeister et al., 2020) techniques driven by observations of e.g. planetary mass, radius, love number and
 425 stellar metallicity. Knowledge of surface composition e.g. via reflection spectroscopy could provide hints on
 426 mantle convection. For example active plate tectonics on Earth produces continental crust mainly in the form of
 427 granite (see discussion in Herbort et al., 2020, their section 3.2). Hu et al (2012) analyzed detectability of
 428 reflection and thermal emission spectra on "airless Earths" for a range of mineral surfaces including basaltic,
 429 ultramafic and granitoid. Distinguishing the resulting small signals (they suggested a few parts per million
 430 differences in the ratio of planetary to stellar flux for e.g. Kepler 20f) however is likely beyond the reach of JWST
 431 and is more an issue for spectroscopy missions further into the future. Other factors which could influence
 432 outgassing include the amount of water in the interior which could affect mantle convection. The water content
 433 of Earth's mantle is not well constrained, ranging from (~0.2 to 3.0) Earth ocean masses (Ohtani, 2020) and is not
 434 known for rocky exoplanets. Recent works (e.g. Namouni and Morais, 2020) suggest that high inclination
 435 Centaurs in our Solar System could have an interstellar origin so could represent the first opportunity to constrain
 436 the building blocks of exoplanets, although such a task is very challenging.

437 Another interesting effect impacting outgassing is the change in the mantle oxidation state (oxygen
 438 fugacity) over time (see e.g. Gaillard et al, this issue; Kadoya et al., 2020; Gaillard et al, 2015) which can in turn
 439 depend on global processes which change the Earth's redox balance and influence outgassing. Observational
 440 constraints of mantle composition (hence fugacity) in an exoplanet context are however weak as stated above.
 441 Over time, disproportionation reactions ($3\text{Fe}^{2+} = \text{Fe}^0 + 2\text{Fe}^{3+}$) in the interior associated to the oxygen-friendly
 442 nature of minerals growing in the transition zone and lower mantle (Frost and Mc Cammon, 2008) that may
 443 induce an oxidation of the upper mantle. This would however be conditioned by the efficient removal of the
 444 produced metallic iron (Fe^0) into the forming core and by the efficiency of global convection in mixing lower and
 445 upper mantle materials. These mass transfer processes are in turn conditioned by the establishment of plate
 446 tectonics representing an efficient convection regime at planetary scale. In brief, the physical status of the planet
 447 interior (style of convection, mantle size) and the chemical state, which rules the efficiency of mantle outgassing,
 448 are intimately intermingled. This implies that planetary mass and outgassing could be somehow related. Broader
 449 relationships exist between planetary interiors and surficial processes. For example, in the upper atmosphere,
 450 loss to space of atomic hydrogen from e.g. water photolysis escapes to space, must leave behind oxygen-enriched
 451 atmosphere, leading to oxidizing continental and seafloor weathering, which if introduced in the mantle by
 452 subduction processes could influence its redox state and outgassing efficiency.

453 Can we test the above feedbacks - proposed by theory and occurring between e.g. atmospheric escape
 454 and the planetary interior - in an exoplanetary context with observables? Regarding escape, an evaporating tail
 455 can form in the trailing planetary limb which could influence the transit lightcurve duration and shape e.g. in the
 456 Lyman-alpha for escaping H-atoms. Oza et al. (2019) summarize spectroscopic detections in the exospheres of
 457 hot Jupiters. Chen et al. (2020) discuss detection of sodium, magnesium and H in the hot exosphere of WASP-
 458 52b and review species detections in the exoplanetary exospheres. Ehrenreich (2015) estimated from transit
 459 observations escape rates of (10^8 to 10^9) g/s for the warm Neptune GJ436b. For the potentially rocky SEs in the
 460 TRAPPIST-1 system, Bourrier et al., (2017) estimated H-escape rates of (4.6, 1.4, 0.6) $\times 10^7$ g/s for TRAPPIST-b,c,e
 461 respectively based on Lyman-alpha transit data obtained with HST. Whether the presence of a magnetic field
 462 increases or decreases atmospheric escape rates is debated (see Dehant et al. 2019, their section 4.2). Exoplanet
 463 science could soon actively contribute to this debate. Proposed techniques involving radio emission and
 464 polarimetry to constrain exoplanetary magnetospheres are under discussion (e.g. Zarka et al., 2019). Proxy
 465 approaches have provided first constraints e.g. magnetohydrodynamic simulations needed to reproduce
 466 observed excursions in peak brightness to the east and the west of the substellar point on the hot Jupiter HAT-
 467 P-7b, required a planetary magnetic field of at least 6 Gauss (Rogers, 2017) (compared with ~0.5 Gauss on Earth's
 468 surface). Cauley et al., (2019) estimated strong magnetic fields in the range (20-120) Gauss for four HJs based on
 469 measurements of the Calcium II K line. The potential role of escape in atmospheric evolution is discussed in
 470 section 4.3 below.

471 How central interior processes such as mantle convection, plate tectonics, outgassing etc. respond to
 472 changing planetary mass such as for SEs is still a subject of debate (see e.g. Noack et al., 2017; Stamenkovic and
 473 Breuer, 2014; Fratanduono et al., 2018), but this brief description shows that the style of geo(exo)dynamics is

474 pivotal in ruling the nature of outgassed atmosphere. Godolt et al. (2019) modeled rocky planets in the HZ of
 475 early M-dwarf stars which have very long active pre-main sequence phases. Their work suggested that planetary
 476 *regassing* could be important for re-instating habitability after the long (~1Gyr) intense (~ $\times 10$ -1000 EUV of the
 477 modern Sun).

478 Regarding delivery of *water* and other volatiles in exoplanetary systems, some key issues are e.g.
 479 identifying the main processes affecting planetary formation and orbital migration (see discussion in Morbidelli
 480 and Raymond, 2016); the extent of turbulent mixing in the disk (Furuya et al., (2013); determining the position
 481 of the water, ammonia and carbon dioxide ice lines (see e.g. Pinilla et al., 2017). The role of dynamical
 482 perturbations [e.g. the “Grand Tack” (Jacobson and Morbidelli, 2014)] which may be important for delivering
 483 volatiles to terrestrial planets which form dry, is not well known for different exoplanetary systems as a function
 484 of stellar and exoplanetary properties of e.g. exo-Jupiters and exo-Saturns. Note that these objects are expected
 485 to be discovered by the ongoing Gaia mission. Regarding mini gas planets, water-dominated atmospheres are
 486 favored thermodynamically ($T > \sim 500\text{K}$, $P > \sim$ a few bar) for solar metallicities of $\sim \times 1000$ (Moses et al., 2013, their
 487 Figure 4). More model formation studies are required investigating the effect of impacts upon atmospheric
 488 delivery and escape as a function of disk and planetary parameters. Direct observations of impact-driven delivery
 489 in exoplanetary atmospheres are not available. Next generation missions however observing dust distributions
 490 in protoplanetary and debris disks, as proposed for the Wide-Field Infrared Survey Telescope (WFIRST) (Nuecker
 491 et al., 2016; Douglas et al., 2018) could however help constrain bombardment rates of early exoplanets by
 492 asteroids which could ultimately help improve the planetary formation models.

493 Regarding *CO₂ atmospheres*, the presence of an Earth-like ocean with active plate tectonics and a
 494 hydrological cycle could enhance CO₂ removal via washout, formation of carbonate and subduction. For weak
 495 weathering cases without plate tectonics, e.g. Foley and Smye (2018) suggested possible runaway CO₂ scenarios.
 496 Responses of CO₂ on rocky exoplanets are generally challenging to predict, being subject to potentially complex
 497 process in the carbon cycle which are mostly unconstrained in an exoplanetary context. Climate stabilizing cycles
 498 are sensitive to many factors including the land-sea mask (e.g. Lewis et al., 2018) and planetary orbital
 499 parameters (Williams and Pollard, 2002). Regarding exoplanets CO₂ has been detected for several planetary
 500 atmospheres (mainly HJs) and JWST will aim to expand knowledge of this species in terrestrial-type atmospheres
 501 (Greene et al., 2016). Obtaining observational hints for oceans (e.g. Robinson et al., 2014) and surface minerals
 502 (see e.g. Hu et al., 2012; Cui et al., 2018, as discussed) are however challenging. Regarding mini gas planets, CO₂
 503 atmospheres are favored thermodynamically ($T > \sim 500\text{K}$, $P > \sim$ a few bar) for solar metallicities of $\sim \times 10,000$ (Moses
 504 et al., 2013, their Figure 4).

505 Regarding *N₂ atmospheres*, global sources and sinks are not well known (see e.g. Lammer et al., 2019;
 506 Wordsworth, 2016). Numerous processes such as volatile delivery (Hutsemékers et al., 2009), outgassing,
 507 lightning, cosmic rays and biological activity all play a role. Further exoplanetary studies are required to establish
 508 which key processes affect atmospheric N₂ evolution (see also section 5.7). Direct spectral observations of N₂ in
 509 exoplanetary atmospheres are currently lacking since its spectral features are weak. Schwieterman et al. (2015)
 510 discussed constraining nitrogen abundances via spectral absorption from N₂-N₂ collisional pairs. Oklopčić et al.
 511 (2016) discussed identifying N₂ and H₂ via so-called ghost line features in Raman spectroscopy. These signals
 512 however correspond to changes of up to a few percent in planetary geometric albedo in the UV so are beyond
 513 the reach of present day missions.

514 Regarding *O₂ atmospheres*, e.g. Gumsley et al. (2017) discuss relevant processes on Early Earth such as
 515 changes in carbon burial rates, mantle redox, biological activity etc. which could influence atmospheric oxygen
 516 abundance. Lingam and Loeb (2019) review the potential for photosynthesis on Earth-like planets. Abiotic O₂
 517 production involving e.g. water photolysis followed by hydrogen atom escape (Luger and Barnes; 2015; Tian,
 518 2015b; Wordsworth et al., 2018) or via CO₂ photolysis followed by self-reaction of oxygen atom (Gao et al. 2015,
 519 Tian et al., 2014) is an expanding field. Note however that NO_x and HO_x species (as on Mars) and additionally
 520 ClO_x (as on Venus) can act as efficient catalysts to facilitate the formation of CO₂ from CO and O as discussed
 521 above. In this case, the N₂, O₂, H₂O and UV amounts in the planetary atmosphere (required to form NO_x and
 522 HO_x) could become important. Grenfell et al. (2018) suggested that atmospheric O₂ abundances can be upper-
 523 limited by explosion-combustion. Theoretical studies (e.g. López-Morales et al., 2019; Rodler and López-Morales,
 524 2014) suggested that several tens of transits are needed with the ELT to detect atmospheric O₂ assuming a close-
 525 by transiting Earth-like atmosphere. Assuming an Earth-like atmosphere on our (non-transiting) neighbor
 526 Proxima Centauri-b would require about 55 hours (assuming R=150,000) ELT observing time (Hawker and Parry,
 527 2019) to detect the atmospheric O₂ A-band in reflected light. Fauchez et al., (2020) suggested that atmospheric
 528 O₂ could be detected via a relatively strong collision-induced absorption feature in the mid/far-infrared (6.4
 529 microns) and may thus be accessible with JWST.

530

531 3.5 Hydrogen (H₂) and Helium (He) atmospheres

532 ProtoEarth and ProtoVenus grew to (50-75%) (Lammer et al., 2018 and references therein) of their
 533 present planetary mass by ~ 10 Myr and accreted thereby (0.1-10%) M_{Earth} hydrogen envelopes i.e. up to a factor
 534 of $\sim 10^5$ times present Earth's atmospheric mass, after which time the gas in the protoplanetary disk had mostly
 535 evaporated. Earth's primordial light atmosphere was likely formed mainly by impact-induced volatile degassing
 536 but also by direct gravitational accretion of gas from the disk (Abe, 2011). Escape processes driven by uncertain,
 537 early XUV evolution from the star are likely important for deciding timescales and to which extent the primordial
 538 atmosphere is lost (e.g. Kislyakova et al., 2015).

539 3.5.1 Jupiter, Saturn, Uranus and Neptune

541 Table 4 shows the composition by volume of the dominant atmospheric species (H_2 and He) for the giant
 542 planets in the Solar system compared with the Solar Values:

Species	Solar	Jupiter	Saturn	Uranus*	Neptune*
Hydrogen (H_2)	0.912	0.897	0.963	0.85	0.80
Helium (He)	0.085	0.102	0.033**	0.15	0.19

544 Table 4: Fractional composition by volume for the Sun (Grevesse et al., 2007), Jupiter and Saturn
 545 (Bagenal et al., 2004) and Uranus and Neptune (Schmude, 2008). *Middle atmosphere measurements.

546 **Jupiter and Saturn** - small differences between Jovian and Solar composition in Table 4 are suggested to arise
 547 due to helium differentiation in Jupiter's core. First-order phase transitions from molecular to metallic hydrogen
 548 could also affect bulk composition (see e.g. Guillot, 1999). The Cassini mission considerably advanced knowledge
 549 of dynamical and temperature responses on Jupiter (e.g. Flasar et al., 2004) and Saturn (Dyudina et al., 2008).
 550 Helium amounts determined from this mission (Koskinen and Guerlet, 2018) suggest more abundant values,
 551 $\text{vmr}_{\text{He}}=0.09$ in the lower atmosphere compared with the earlier data shown in Table 4. Atmospheres of Jupiter
 552 and Saturn feature complex hydrocarbon chemistry (e.g. Smith and Nash, 2006) and cloud formation via e.g.
 553 phosphorous, water, and sulphur-containing species (Atreya et al., 1999).

554 **Uranus and Neptune** – likely have small rocky cores and are generally carbon-enriched compared with Jupiter
 555 and Saturn (Ali-Dib et al., 2014; Mousis et al., 2018). Recent advancements have been made in understanding
 556 the circulation (Orton et al., 2014) and brightness (Nettelmann et al., 2015) of Uranus as well as the composition
 557 (e.g. Moreno et al., 2017) of Neptune. Hydrocarbon photochemical responses on the ice giants are discussed in
 558 Moses et al., (2019).

559 Atreya et al., (2020) comprehensively reviewed planetary composition, structure, origins and potential missions
 560 for the Solar System Gas and Ice Giants.

561 3.5.2 Exoplanetary context

562 When interpreting the bulk composition of the Solar System's giant planets, it is interesting to separate
 563 the influence of formation timescales and migration on the one hand, from that of planetary parameters such as
 564 mass, radius and core properties on the other hand. Studying cool exoplanetary giant planets in future will be
 565 useful in this regard. Helium detections in exo-Neptunes such as HAT-P-11b (e.g. Mansfield et al., 2018; Allart et
 566 al., 2018) are relevant in this respect. Hu et al. (2015) modeled helium exo-atmospheres on warm Neptunes such
 567 as GJ436b. Regarding atmospheric hydrocarbons, model studies (Moses et al., 2018) suggest summer-winter
 568 asymmetry due to photochemical responses in the atmospheres of the giant planets in the Solar System which
 569 they suggested could be tested in an exoplanetary context using the JWST if suitable cool giant exoplanet targets
 570 are found. Regarding (Ultra) Hot Jupiters [(U)HJs], their atmospheric composition and detection are reviewed in
 571 e.g. Maldonado et al. (2018) and Madhusudhan (2019); their atmospheric structure in Laughlin (2018) and
 572 transport in e.g. Komacek and Showman (2016). Grenfell et al. (2020) summarized potential atmospheric
 573 observations of HJs and nearby SEs using the planned color filters on the PLATO fast cameras. We do not however
 574 discuss (U)HJs in detail here since our focus in the present work lies with the smaller mass terrestrial-type
 575 exoplanets

576 **3.6 Summary** – the Solar System may be atypical in some respects. For example it features neither mini gas
 577 planets nor SEs which may be rather common in the Universe (Burke et al., 2015). Nevertheless, studying the
 578 Solar System provides valuable lessons regarding e.g. volatile budgets, delivery, magma oceans, outgassing and
 579 steam atmospheres for the inner terrestrial planets as well as lessons regarding the formation and composition

586 of outer gas planets. This can be an invaluable exercise when considering the potential diversity of exoplanetary
 587 atmospheres.

588

589 **4. Key Phenomena anticipated to affect Exoplanetary Atmospheric Diversity**

590

591 **4.1 Elemental abundances in the protoplanetary disk**

592 Molecular clouds (MCs) are one of the most investigated phenomena in the interstellar medium, yet the
 593 main mechanisms by which they form, evolve and collapse are not well understood (see overview by Vázquez-
 594 Semadeni et al., 2006). MCs typically contain ~90% H₂ gas with masses in the range $\sim(10^2\text{-}10^6)M_{\odot}$ and
 595 temperatures (10-50K). Differential rotational rates in the branches of the Milky Way can lead to MC rotation. At
 596 the rotational equator of the MC, the outward centrifugal force balances the inward gravitational force. Along
 597 the MC rotational axis however, the unbalanced gravitational force leads to inward transport of material so that
 598 the MC flattens into an accretion disk (Maeder, 2009). Observations of evolving disks by the Atacama Large
 599 Millimeter Array (ALMA) telescope have greatly advanced the field (Matrà et al., 2018).

600 Metallicity distribution functions across the Milky Way were discussed e.g. in Nidever et al. (2014) and
 601 Hayden et al. (2015). The latter study suggested (Fe/H) values ranging from -0.5 to 1.5 for a sample of ~70,000
 602 stars. Variations in elemental abundances across the protoplanetary disk, however, depend on uncertainties in
 603 the dynamics and timescales of e.g. disk collapse, disk mass, dust-to gas ratios and photochemical effects.
 604 Predicting the position of disk snowlines and the resulting variation of planetary elemental ratios such as (C/O)
 605 and (C/H) in the gas and solid phases helps constrain whether such species were accreted as dust or gas during
 606 planetary formation. This can in turn help differentiate between proposed planetary formation mechanisms such
 607 as the 'gravitational instability' as opposed to the 'core accretion' mechanism (see Venturini and Helled, 2017).
 608 It can also provide information on migration rates and constrain location(s) in the disk at which the forming
 609 planet accreted its metals (see e.g. Booth et al., 2017; Krivov and Booth, 2018; Lin et al., 2018; Booth and Ilee,
 610 2019). Dorn et al. (2015) used stellar elemental data and planetary mass-radius observations to constrain core-
 611 mantle radii and discussed future applications of this technique to constrain exoplanetary atmospheres and
 612 oceans. Several theoretical studies have varied metallicity and modeled the resulting atmospheres assuming
 613 chemical equilibrium (see review by Madhusudhan et al., 2016 and references therein). Moses et al., (2013)
 614 calculated the effect of varying metallicity values from x1 to x10⁴ Solar in hot Neptunes and calculated (their
 615 Figure 5) atmospheres ranging from H₂ and H₂O for medium-range (x1-x10² Solar) metallicities and forming N₂
 616 atmospheres for higher metallicities. For metallicities greater than x100 Solar, they noted CH₄-dominated
 617 atmospheres for temperatures less than 600K and CO-dominated atmospheres for temperatures greater than
 618 800K. Hu and Seager (2014) varied assumed mole fractions, X_H (from 0 to 1) and (X_C/X_O) (from 0 to 1 to 10) in a
 619 model study of the SE GJ1214b. Their results suggested atmospheres ranging from e.g. highly oxidized (e.g. O₂-
 620 dominated) at low (C/O) changing to highly reduced (CH₄ and other hydrocarbons such as C₂H₂ (ethyne) and C₂H₄
 621 (ethene) at high (C/O)).

622

623 **4.2 Variations in initial interior volatile reservoirs and outgassing**

624 Processes which influence outgassing can be broadly considered as follows. First, the initial (local)
 625 volatile concentration delivered to the planet, which is related to the concept of feeding zones (Grewal et al.,
 626 2019) and the changes in orbital trajectory during planetary accretion (see 3.4.4). Then, the C-H-O-N-S elements
 627 which are supposedly outgassed from the planetary interior to form the atmosphere are not always volatiles.
 628 Recent research efforts (Hirschmann 2012; Rohrbach et al., 2014; Dasgupta and Grewal, 2019; Malavergne et al.,
 629 2019) clearly show that these elements can be siderophile or refractory, implying that under certain conditions
 630 or during specific stages in the differentiation of a planet, they are not outgassed from the mantle, but remain
 631 sequestered in the planetary interior. Technically, the effective partitioning of volatiles into the melt depends
 632 on e.g. redox state, melt fraction, composition, temperature and pressure. These parameters are linked to the
 633 exogeodynamics (see 3.4.4) defining the style of planetary internal convection (eg. Noack et al., 2014). On planet
 634 Earth, geochemical constraints indicate that carbon is in the oxidized form of carbonate in the shallow mantle
 635 (ie. <180 km depth) while it is completely in the form of diamond at greater depth (Frost and Mc Cammon, 2008;
 636 Gaillard et al., 2015). This redox transition is critical for the removal of carbon upon mantle melting since only
 637 oxidized carbon can be outgassed while diamond/graphite is refractory. This also has implications on the
 638 speciation of other volatiles like hydrogen, by affecting reduced volatiles such as H₂ and CH₄ (e.g. Dasgupta,
 639 2013). On Mars, oxidized carbon is not expected due to a much reduced mantle; this implies a limited carbon
 640 outgassing from the Martian mantle in comparison to Earth. Finally, the volatility of the C-H-O-N-S (transfer from
 641 melt to gas) is the last condition for outgassing into the atmosphere. Nitrogen and sulfur are not volatile under
 642 the most reduced conditions typical of Mercury for example (Gaillard et al., 2015). Under oxidizing conditions,
 643 however, they can be as volatile as other components (ie. CO₂, CO, H₂O, H₂O). Outgassing CO₂ and CO from the

644 melt is always favored since these are very volatile species. Water is much less volatile than CO₂. This hierarchy
 645 in the volatility implies that the composition of the outgassed mixture from a basalt is chiefly pressure
 646 dependent: at high pressure (~a few tens of bar and above), water is not outgassed, while at low pressure (< 0.1
 647 bar), most of the C-H-O-N-S elements can be outgassed (Gaillard and Scaillet, 2014). In brief, pressure and oxygen
 648 fugacity are the parameters ruling the amount and nature of degassed mixture from a basalt.

649 How could mantle oxygen fugacity have evolved through time on planet Earth? Frost and McCammon
 650 (2008) suggested an oxidized mantle was reached at ~1Gyr after core formation. Li and Lee (2004) and Trail et
 651 al. (2011) provided evidence for constant fO₂ values in the upper mantle over geological time back to 4.3 Ga. A
 652 consensus seems to emerge here, but there remain large uncertainties preventing the used redox proxies to
 653 provide firm conclusion (e.g. Yang et al., 2014). During core-mantle separation, conditions were extremely
 654 reduced implying an atmosphere dominated by H₂ and CO (Hirschmann, 2012; Gaillard et al., 2015). After core
 655 formation, the efficiency of carbon removal into the core influenced the subsequent mantle fO₂ and coeval
 656 atmosphere evolution (Hirschmann, 2012). How oxygen fugacity evolved during the late stage of the magma
 657 ocean appears pivotal (Elkins-Tanton et al., 2008; Elkins-Tanton et al., 2012). Recent efforts link the depth of the
 658 magma ocean to the evolution of its oxidation state and the fate of carbon (Armstrong et al., 2019). It is then
 659 possible that right at the end of the magma ocean stage, the oxygen fugacity of the Earth's mantle was similar
 660 to the present-day one with an oxidized shallow mantle and a deep reduced one. But such planetary systems
 661 may not always be considered as a closed system: Over geological timescales, (a) prolonged hydrogen
 662 atmospheric escape (involving water photolysis followed by removal of hydrogen to leave behind oxygen which
 663 can be weathered into the surface), (b) delivery of oxidized late veneer material and (c) subduction of oxidized
 664 mineral could also drive mantle oxidation (Kasting et al., 1993). Orders of magnitude difference in the outgassed
 665 mass of volatiles can arise depending on the processes listed above.

666 **4.3 Extreme atmospheric escape**

667 Atmospheric escape can be limited by diffusion (depending on e.g. atmospheric scale height of different
 668 species and the concentration of escaping species) or energy (depending on incoming XUV or high energy particle
 669 fluxes from the central star). Regarding atmospheric escape in the modern Solar System, Jupiter is sufficiently
 670 massive and far from the Sun to prevent efficient escape in virtually any form. Regarding Venus, Earth and Mars,
 671 escape processes have been reviewed by numerous works e.g. Shizgal and Arkos (1996). In the early Solar System,
 672 atmospheric escape on Venus, Earth and Mars was discussed in e.g. Lammer et al. (2018). On Pluto, Zhu et al.
 673 (2014) suggested energy-limited escape which hydrodynamic treatments under-estimate by ~13% (see also Hoey
 674 et al., 2017). The New Horizon observations suggest that theoretical calculations of atmospheric escape on Pluto
 675 generally over-estimate observed losses.

676 Regarding exoplanets, numerous earlier works modeled hydrodynamic escape on Hot Jupiters (see Tian,
 677 2015 and references therein). Tripathi et al. (2015) applied a 3D hydrodynamic model which suggested day-night
 678 asymmetries in outflow for tidally-locked Hot Jupiters. Weber et al. (2017) modeled plasma conditions near the
 679 exobase of Hot Jupiters. Insight into planetary formation and the role of escape has been revealed by
 680 observational studies of the so-called Neptunian desert (e.g. Mazeh et al., 2016) and the "radius" or "Fulton" gap
 681 (Fulton et al., 2017; Owen and Wu, 2017; Lehmer and Catling, 2017; Jin and Mordasini 2018; Gupta and
 682 Schlichting, 2019) for close-in planets. Lammer et al. (2013) suggested blowoff and Roche lobe overflow could
 683 occur for SE atmospheres. Tian (2009, 2013) modeled planetary upper atmospheres containing heavy molecules
 684 such as N₂, O₂ and CO₂ under strong XUV radiation. Johnstone et al., (2015) and Erkaev et al., (2016) modeled
 685 the important role played by XUV for escape processes for SEs with hydrogen dominated atmospheres.

686 Regarding rocky exoplanets orbiting M-dwarf stars, an important question is to what extent they can
 687 retain their atmospheres. Tian and Ida (2015) suggested that Earth-like planets with Earth-like oceans could be
 688 rare for cool star systems due to efficient water loss over the extended pre-main sequence. The model study by
 689 Owen and Mohanty (2016) included an updated escape model with improved radiative cooling and transition
 690 between hydrodynamic and ballistic regime, which suggested that large primordial hydrogen envelopes may
 691 survive the early, extreme early EUV phase for rocky worlds around cool stars. Dong et al. (2018) modelled the
 692 TRAPPIST-1 system and suggested ion escape rates (10²-10³) times faster than that on Earth assuming an initial
 693 one bar atmosphere with Venus-composition. Their modelled stellar winds were ~three times faster than the
 694 Sun for the same star-planet distance. Their work suggested complete atmospheric removal for the inner
 695 TRAPPIST-1 planets for surface pressures up to ~10bar. They noted that more work is required to characterize
 696 the properties of the incoming stellar wind. It should also be noted that the impact of rapid loss on the energy
 697 budget of the underlying planetary upper atmosphere is not considered in Dong et al. (2018) and thus their loss
 698 rate could be more limited by the energy conservation principle proposed in Tian (2013). Kubyshkina et al.,
 699 (2018) presented an updated method based on gridded analytical fits to replace the energy-limited formula
 700 commonly employed to estimate atmospheric escape. Tian et al. (2018) reviewed recent progress in
 701

702 understanding the evolution of stellar XUV and the relevance for water loss on terrestrial exoplanets. Johnstone
 703 et al. (2018) developed a flexible 1D upper atmosphere escape model validated for Earth and Venus to model
 704 the effect of e.g. stellar XUV evolution. Applying this model to terrestrial-type planets orbiting early, active solar-
 705 like stars (Johnstone et al., 2019) suggested Earth-like atmospheres cannot form due to transonic hydrodynamic
 706 escape of e.g. C and O.

707

708 **4.4 Clouds**

709 Clouds are common features in planetary atmospheres throughout the Solar System (see e.g. Taylor,
 710 2010). Cloud microphysical processes include homogeneous nucleation, heterogeneous nucleation (occurring on
 711 condensation nuclei such as aerosol and dust particles), coagulation (growth) and sedimentation. Complex
 712 climate feedbacks exist between clouds, radiation and transport which are still being unraveled in Earth's
 713 atmosphere (see e.g. Ceppi and Hartmann, 2015).

714 In exoplanet science, the central role of clouds and hazes is becoming more and more apparent. The
 715 presence of clouds can flatten the transmission spectra of Hot Jupiters (see e.g. Parmentier et al., 2016; Wakeford
 716 et al., 2016; Powell et al., 2018). Regarding hot SEs, Mahapatra et al., (2017) investigated the potential role of
 717 atmospheric mineral-based clouds. Schaeffer and Fegley, (2009) suggested clouds consisting of sodium or/and
 718 potassium-containing minerals for hot SEs which (for favourable candidates) could be observable with current
 719 facilities.

720 Regarding warm SEs, Kreidberg et al. (2014) suggested the presence of clouds in the atmosphere of
 721 GJ1214b in order to be consistent with transit spectroscopy data (see also Charnay et al., 2015; Mollière et al.,
 722 2017; Gao and Benneke (2018). Morley et al. (2015) modelled cloudy thermal emissions and reflection spectra
 723 in SE atmospheres. Kawashima et al. (2019) performed feasibility studies for spectral detections by the James
 724 Webb Space Telescope (JWST) assuming clouds and hazes on GJ1214b, GJ 436b, HD 97658b, and Kepler-51b.
 725 Benneke et al. (2019) suggested that Mie-scattering by clouds is responsible for the flat spectrum they observed
 726 for GJ3470b at visible and near infrared wavelengths. The impact of such clouds should decrease for observations
 727 at longer wavelengths.

728

729 **5. Case Studies of Exoplanetary Atmospheres**

730

731 **5.1. Magma Ocean Worlds**

732 A magma ocean (MO) planet features a molten mantle without a planetary crust and surface
 733 temperatures in the range $\sim(1000-2000\text{K})$ which is generally sufficient to melt silicate minerals depending on
 734 their composition. Such conditions can be reached temporarily e.g. after the planetary accretional phase, or
 735 permanently e.g. for close-orbiting terrestrial exoplanets as discussed in Hamano et al. (2013) and Nikolaou et
 736 al. (2019). A number of potential MO exoplanets have been identified, such as Corot-7b, 55 Cancri e, TRAPPIST-
 737 1b and Kepler 10b (e.g. Hammond and Pierrehumbert, 2017; Henning et al., 2018; Nikolaou et al., 2019 and
 738 references therein).

739 Exoplanetary model studies of MO atmospheres focused on e.g. interior-atmosphere coupling,
 740 atmospheric composition, cooling processes and the length of the MO phase (see e.g. Lebrun et al., 2013). Kite
 741 et al. (2016) suggested MO world atmospheres close to vapor-pressure equilibrium determined by fractional
 742 vaporization and surface-interior exchange. Marcq et al. (2017) applied a coupled interior-atmosphere model
 743 simulating $\text{H}_2\text{O}-\text{CO}_2$ atmospheres which confirmed that the outgoing LW blanketing effect saturates at the
 744 Nakajima limit (Nakajima et al., 1992) of $\sim 280 \text{ Wm}^{-2}$ (and $\sim 40\%$ less for atmospheres assuming clouds) for
 745 scenarios with 300 (100) bar surface pressure of H_2O (CO_2). They suggested the limit breaks down for surface
 746 temperatures above 1690K (1970K) for scenarios with (without) clouds, although these values depend on
 747 atmospheric composition and mass. Breakdown occurs as successively hotter planetary surfaces emit radiation
 748 at successively lower wavelengths. Lupu et al. (2014) modeled atmospheric composition and evolution of post
 749 giant impact atmospheres on Earth-like planets. Nikolaou et al., (2019) applied a coupled interior-atmosphere
 750 model to discuss whether a sample of potential MO exoplanets could lie in temporary ("evolutional MO") or
 751 permanent MO states depending on e.g. albedo and incoming stellar radiation.

752 Atmospheric species on MO worlds can be removed directly by surface ingassing e.g. for noble gases as
 753 indicated by studies of mantle $^3\text{He}/^{22}\text{Ne}$ preserves (Tucker and Mukhopadhyay, 2014). Sharp (2017) suggested
 754 ingassing during the MO phase could represent a major mechanism for delivery of volatiles into the interior (see
 755 also Olson and Sharp, 2018). Wu et al. (2018) discussed mantle acquisition of noble gases, H_2 and H_2O during the
 756 MO phase. Wordsworth (2016) discussed thermolytic dissociation or/and dissolution of nitrogen-containing
 757 species into the MO. Kite et al (2019) suggest that ingassing of H_2 during the MO phase may be responsible for
 758 forming the steep decrease in the planetary occurrence rate between 3-4 Earth radii.

759

760 5.2 Steam Atmospheres

761 A massive steam atmosphere e.g. with hundreds to thousands of bars pressure at the surface can be
 762 outgassed during crustal formation at the end of the MO phase on terrestrial-type planets. Subsequent cooling
 763 could then lead to ocean formation via condensation. Elkins-Tanton (2011) noted that planetary formation
 764 models suggest SEs could commonly acquire their oceans via such a mechanism. On the other hand, if the
 765 planet's incoming stellar radiation is strong, this could result in a prolonged steam atmosphere phase with
 766 atmospheric desiccation via water photolysis followed by escape. Alternative to steam outgassing, it is feasible
 767 that so-called waterworlds (Léger et al., 2004) could evaporate their water inventory and form massive steam
 768 atmospheres if they migrate sufficiently far inwards. Kite and Ford (2018) suggested that waterworlds could be
 769 common and modeled their habitability limits. Goldblatt (2015) modeled the dependence of steam atmosphere
 770 amount and duration upon planetary mass and incoming stellar radiation. Fegley et al. (2016) suggested that
 771 exoplanetary steam atmospheres could dissolve magnesium, iron and alkali metal oxide minerals which could
 772 potentially modify their surface composition. The model study of Pluriel et al. (2019) suggested high bond
 773 albedos (~ 0.8) for steam exo-atmospheres ($T_{\text{surf}} \sim 1000\text{K}$) (an effect associated with clouds) and medium bond
 774 albedos (~ 0.5) for hotter steam atmospheres ($T_{\text{surf}} \sim 2000\text{K}$) where gas absorption becomes more important.

775 Steam atmospheres are also investigated in the context of determining via model studies the inner
 776 habitable zone boundaries (HZ). Earlier works e.g. Kopparapu et al. (2013) noted the importance of employing
 777 detailed, up-to-date line-lists for water when determining the inner HZ. Leconte et al., (2013) investigated
 778 simulating in 3D the effect of under-saturated descending Hadley cells. A summary of 1D and 3D modeling studies
 779 of steam atmospheres near the inner HZ, including important cloud feedbacks are summarized in Godolt et al.,
 780 (2016) and references therein. Thomas and Madhusudhan (2016) noted that thick steam atmospheres could
 781 increase the radii of water-rich planets by up to several tens of percent - which could be used as an observational
 782 indicator for the volatile content on sampled rocky exoplanets by future missions (see also Turbet et al., 2019
 783 and Turbet et al., 2020).

784

785 5.3 Oxygen Atmospheres

786 The global oxygen cycle (on modern Earth) is influenced by processes extending over the interior-
 787 lithosphere-biosphere-atmosphere system (see e.g. Petsch, 2003; Catling and Claire, 2005).
 788 Regarding *sources*, the main net source of atmospheric O_2 is via subductive burial ($\sim 12 \text{ Tmol C/yr}$; Holland, 2006)
 789 occurring mainly near continental margins (Hartnett et al., 1998). This process regulates how much O_2 from
 790 photosynthesis (forming O_2) can enter the atmosphere by subducting organic material, making it unavailable for
 791 respiration (destroying O_2). A minor source of O_2 ($3 \times 10^8 \text{ molecules cm}^{-2} \text{ s}^{-1}$) on modern Earth, occurring ~ 100
 792 times slower than burial; see Yung and DeMore, 1999) is via atmospheric escape which proceed via photolysis of
 793 water followed by escape of H then self-reaction of the resulting O to form O_2 . This O_2 source could however be
 794 important in Early Earth type environments and on terrestrial-type exoplanets (see below).

795 Regarding *sinks*, the main sinks of atmospheric O_2 (on modern Earth) include (a) atmospheric reaction with
 796 reduced outgassed species such as CH_4 and H_2 (resulting in a net sink of $\sim 1\text{-}3 \text{ Tmol/yr O}_2$; Catling and Claire, 2005),
 797 (b) metamorphic reactions of O_2 directly on hot rock surfaces ($\sim 2.5 \text{ Tmol/yr O}_2$; Catling and Claire, 2005)
 798 associated with volcanic activity, and (c) weathering ($\sim 16 \text{ Tmol/yr O}_2$, Holland, 2002) occurring via O_2 dissolving
 799 in rain followed by chemical reactions on surface rock. Earlier, mainly box model studies have investigated O_2
 800 evolution over geological timescales on Earth (see Lenton and Watson, 2000; Berner, 2001). Lacking however in
 801 the literature are evolutionary studies with recent, coupled climate-photochemical models. Gebauer et al. (2017)
 802 and Gebauer et al. (2018) investigated processes affecting atmospheric oxygen on Earth and on Earth-like
 803 exoplanets respectively. On Earth, O_2 levels have remained stable at $\sim 21\%$ for several hundred Myr. There is no
 804 firm understanding of the feedback mechanisms which maintain long-term regulation of O_2 (Lasaga and Ohmoto,
 805 2002).

806 Regarding exoplanets, lessons from Earth science suggest that processes affecting O_2 are numerous and
 807 diverse. Regarding exoplanetary O_2 *sources*, (a) the development of photosynthesis was likely an evolutionary
 808 singularity in the history of our planet, as reviewed by Fischer et al., (2016). Gale and Wandel (2017) (building on
 809 earlier work of Kiang et al., 2007) investigated the potential of Earth-like worlds orbiting M-dwarf stars to support
 810 exo-photosynthesis. Meadows et al., (2018) discussed interpreting O_2 as an atmospheric biosignature in the
 811 context of its environment. Lingam and Loeb (2019) discussed the impact of exo-photosynthesis and its possible
 812 variants upon the atmospheres of Earth-like planets. Ward et al. (2019) review factors affecting atmospheric
 813 oxygen in the Solar System and beyond. The above studies assume that Earth-like planets in the HZ of M-dwarf
 814 stars can retain atmospheres although some works e.g. Airapetian et al. (2017) suggested that ion escape could
 815 efficiently remove Earth-like atmospheres on such worlds within tens to hundreds of Myr. Regarding (b) the O_2
 816 source due to H-escape discussed above, clearly this process is favored for smaller-mass exoplanets orbiting stars
 817 active in XUV. Abiotic gas-phase reactions could also influence atmospheric oxygen in Earth-like planets.

818 Although not significant in Earth's modern atmosphere, abiotic production of O₂ could proceed efficiently in e.g.
 819 CO₂-dominated atmospheres via CO₂ photolysis whereby the resulting O-atoms self-react to form molecular
 820 oxygen. The abiotic production is strongly disfavored by the presence of hydrogen oxides (HOx) and nitrogen
 821 oxides (NOx). These species are produced in Earth-like atmospheres e.g. from lightning and cosmic rays which
 822 release HOx and NOx by breaking down their reservoir species such as nitric acid and water. HOx and NOx
 823 disfavor abiotic O₂ production by driving catalytic gas-phase cycles which convert atomic O (from CO₂ photolysis)
 824 back into CO₂. In an atmosphere with a high concentration of O₂ from CO₂ photolysis, the O₂ is likely to coexist
 825 with a high concentration of CO, therefore simultaneous observation of CO and O₂ could therefore be an efficient
 826 method to distinguish the abiotically-produced from the biological O₂ (Wang et al. 2016). The mechanism was
 827 discussed in Selsis et al. (2002); Tian et al., (2014); Gao et al., (2015) and Luger and Barnes (2015).

828 Regarding exoplanetary O₂ *sinks*, these likely depend upon (a) outgassing in both amount and
 829 composition of reduced compounds. These depend in turn upon mantle dynamics and the ability of the interior
 830 to absorb compounds e.g. during core formation, as discussed above. The metamorphic sink (b) will be favored
 831 on exoplanets with extended hot rocky surfaces. The weathering sink (c) will be favored on exoplanets with
 832 strong hydrological cycles and extensive, long-term continental coverage which are currently unknown
 833 parameters. Timescales for establishing the continents calculated by models for early Earth vary from several
 834 hundred Myr (fast growth) to several thousand (slow growth) Myr (Taylor and McLennan, 1985) depending on
 835 uncertainties in the dynamics and heat distribution in the mantle. Grenfell et al. (2018) suggested an upper limit
 836 sink for O₂ on Earth-like planets (depending on T,p, composition) due to explosion-combustion initiated by cosmic
 837 rays or lightning. Wordsworth et al. (2018) performed modeling studies of GJ1132b, an Earth-sized planet
 838 transiting an M-dwarf star. Results suggested O₂ atmospheres could vary over a large range - from tenuous
 839 atmospheres up to very thick (several thousands of bar at the surface) depending mainly on the initial planetary
 840 water budget assumed. Earth-like atmospheres, defined here as (N₂-O₂) dominated were suggested to be
 841 geobiosignatures by e.g. Lammer et al., (2019), Airepation et al., 2017) since their build-up together to significant
 842 values (>tenths of bar surface pressure or more) likely requires life to generate the required redox disequilibrium.
 843 Krissansen-Totton et al. (2016) suggested that strong redox disequilibrium arose on Earth due to the
 844 simultaneous presence of N₂ together with O₂ and liquid water (see also Krissansen-Totton et al., 2018).

845 In summary, the extent and diversity of O₂-dominated atmospheres on Earth-like planets is currently
 846 difficult to estimate. Key uncertainties include the likelihood of photosynthesis occurring beyond the Earth and
 847 upon abiotic processes occurring in-situ in the atmosphere. Whereas biological O₂ formation likely proceeds at
 848 the surface, abiotic O₂ production likely peaks in the atmosphere depending on the trade-off between its
 849 chemical precursors and the availability of UV/XUV. This difference could lead to differing vertical distributions
 850 of O₂ which if measurable could be a means to distinguish the two mechanisms. Strong and protracted outgassing
 851 of reduced compounds together with strong rainout and continental coverage and the presence of plate
 852 tectonics could lead to a reduction in the atmospheric O₂ abundance via weathering. We now apply the above
 853 ideas in order to discuss a current research question.

854

855 **5.3.1 What is the fate of oxygen or/and water during runaway climate processes?**

856 As discussed earlier, for planets that are close to their host stars, a runaway greenhouse could occur and
 857 the planet could develop a dense steam atmosphere with a hot climate for a certain period of time. If there is
 858 adequate UV radiation to dissociate water molecules and the XUV radiation imposed on the planet is strong
 859 enough, rapid loss of H and O will occur. Note that the loss of H has been suggested (Tian, 2015a) reach the ratio
 860 of 2:1 so that net loss of water occurs. If the initial loss of H is more than O, atmospheric O₂ could build up and
 861 lead to more loss of O. If the inventory of water on the planet is massive, it is possible that the planet will remain
 862 a water-rich body with a dense steam atmosphere and an extended H and O envelope for an extended period of
 863 time. Such types of planets do not exist in our Solar System but might be observed in the future in exoplanetary
 864 systems. Observationally these types of planets would be similar to mini-Neptunes except that they have more
 865 oxygen in their extended atmospheres. We note that planets with an extended H and O envelope may also be
 866 experiencing a moist greenhouse state in which the atmosphere is not dense and steamy.

867 The initiation and maintenance of planetary (climate) runaway require an imbalance in climate
 868 feedbacks in which net positive (self-enforcing) feedbacks (e.g. ocean evaporation-greenhouse heating; ice-
 869 albedo) outbalance net negative stabilizing feedbacks (carbonate-silicate cycle; cloud reflection; Planck
 870 emission). Some key processes which could prevent a runaway planet from accumulating O₂ are as follows.
 871 Firstly, O₂ may be absorbed into the magma ocean if the mantle is sufficiently reducing (see e.g. Wordsworth et
 872 al., 2018). Secondly, the surface could remove O₂ via weathering (see 5.3) depending on e.g. mineral composition,
 873 or/and the presence of plate tectonics. Processes one or/and two could have occurred on early Venus and Venus-
 874 like worlds (see Wong et al., 2019). Thirdly, O₂ could rapidly escape in the hydrodynamical regime (see e.g.

875 Bolmont et al., 2017; Johnstone et al., 2019) e.g. if the star is highly active in XUV, as discussed. Modeling studies
876 are required to disentangle the fate of oxygen and water due to runaway climate effects.

877

878 5.4 Methane atmospheres

879

880 5.4.1 What would Titan look like closer to the sun?

881 We discuss here a thought-experiment in which modern Titan is shifted towards the Sun and then
882 consider how the atmosphere would respond. We consider thereby Titan as an example of an icy body
883 (waterworld) which has migrated inwards from beyond the snowline (see e.g. Léger et al., 2004). The potential
884 habitability of waterworlds was discussed in e.g. Goldblatt (2015) and Kite and Ford (2018). A central aim of our
885 thought experiment is to instigate further discussion and to encourage additional modeling studies of
886 atmospheric evolution on these worlds to understand atmospheric diversity. Note that Turet et al., (2018)
887 considered how Titan would evolve if placed at the orbit of the TRAPPIST-1 planets. They concluded that such a
888 warm Titan would likely be efficiently depleted in CH₄ due to strong photolysis. This is favored since CH₄, unlike
889 H₂O, continuously exists in "moist greenhouse" since firstly, it has no atmospheric cold trap being hard to
890 condense, and secondly, it absorbs efficiently in the near infrared which weakens the cold trap.

891 Titan has a cold (94K) surface temperature with ~1.5 bar N₂-dominated atmosphere containing ~1.4%
892 CH₄ in the stratosphere, up to ~5% CH₄ near the surface (Tobie et al., 2005) and thick organic hazes in the middle
893 and upper atmosphere (see e.g. Yung and DeMore, 1999 and references therein). Much was learnt about Titan's
894 atmosphere during the Cassini mission (see e.g. Coustenis et al., 2009). Krasnopolsky (2019) reviews
895 observational and modeling insight. At the start of our thought experiment, instellation begins to increase so
896 that methane in the upper layers is photodissociated e.g. at Lyman-alpha wavelengths to form (in the case of
897 CH₄) a mixture of radicals (C¹D, CH, CH₂, CH₃) and hydrogen (H₂, H) species (see Gans et al., 2011) and their ions.
898 Nitrogen is also dissociated in the EUV into nitrogen atoms and ions. Titan's mass is only 6.7% that of the Earth
899 (~3.3 Earth moons) so that the atomic hydrogen resulting from methane photolysis could be efficiently lost as
900 Titan moves inwards. This mechanism could be especially important for early exo-Titans which migrate inwards
901 when the young central star is active in XUV. With increasing temperatures, evaporation of the lighter (short
902 chain) organic aerosol is generally favored over heavier (long chain) aerosols which condense more easily than
903 their lighter chain counterparts. The climate response of the thick haze is however potentially complex since it
904 could either counteract (amplify) warming from increased instellation by reflecting (scattering) incoming
905 shortwave radiation depending on its composition, shape, size distribution and altitude.

906 An interesting level of instellation is reached in our thought experiment where the surface temperature
907 exceeds $T_{\text{evap(CH}_4\text{)}} \sim 112\text{K}$ at which point liquid methane begins to boil. Lidar data from Cassini (Mastrogiuseppe et
908 al., 2014) suggests Titan's methane-ethane lakes would lead to ~70m mean coverage on Titan's surface but
909 contain only ~1.4% of atmospheric methane. Evaporation would therefore lead to only a modest influx of
910 methane into the atmosphere. This would likely block incoming radiation, strengthen the anti-greenhouse effect
911 and favor haze formation, but increase methane photolysis in the upper layers and hence likely increasing escape
912 rates of hydrogen (a product of methane photolysis). Another interesting level of instellation is reached where
913 water ice or/and ammonia-water layers melt (see e.g. Tobie et al., 2005) which have an estimated mean thickness
914 from 50 to 200km based on Cassini orbital data (see e.g. Hemingway et al., 2013 and references therein). This
915 global melting event could lead to the formation of deep surface oceans containing ammonium hydroxide which
916 has a strongly suppressed freezing point compared to water.

917 Further increasing instellation could eventually lead to evaporation of the NH₃ and H₂O ocean (see Yang
918 et al., 2017). Depending on the UV environment, the H₂O vapor could photolyse to form the hydroxyl (OH) radical
919 which is a strong in-situ sink for atmospheric CH₄, whereas the NH₃ (if not efficiently shielded from UV) would be
920 photolytically removed (see. e.g. Wolf and Toon, 2010). A plausible scenario for the final atmospheric state is
921 therefore mainly N₂ with some water vapor and CH₄ depending on the uncertain initial water inventory and rate
922 of atmospheric escape. Such a habitable state could however be potentially short-lived because of the relatively
923 short timescale of H loss.

924 Although numerous studies have modeled Titan's climate and composition, also with General
925 Circulation Models (see e.g. Lora et al., 2015; Lebonnois et al., 2012) there are much fewer studies investigating
926 Titan's atmospheric response to changing insolation. Lorenz and Lunine (1997) modelled Titan's future
927 atmosphere response as the Sun evolves into a red giant. They proposed an initial insensitivity to increasing solar
928 energy due to the thick organic haze and discussed UV-haze feedbacks as the Sun reddened and weakened in UV
929 output. They also discussed the potential presence of water-ammonia oceans. McKay et al., (1991) discussed
930 potential climate responses on modern Titan due to the net greenhouse heating effect (+15K) which they
931 decomposed into (a) an anti-greenhouse cooling (-9K) due to hazes plus (b) greenhouse heating (+21K) due to
932 collision-induced absorption of N₂-N₂, CH₄-N₂ and H₂-N₂.

933 In an exoplanetary context, since modern Titan's atmosphere originates either directly from the
 934 Saturnian high density disk or/and from cometary impacts early in its history (e.g. Lunine et al., 1998), one can
 935 therefore anticipate exo-Titan atmospheres to consist of N_2 - NH_3 - CH_4 - H_2 gas mixtures depending on e.g. the
 936 location and timescale of formation and the role of cometary delivery. Migration likely depends on numerous
 937 factors such as the timing and location of the object's early growth. The presence of a large primordial H_2
 938 envelope could strongly influence the photochemistry since H_2 participates in "cracking" cycles which shorten
 939 the atmospheric hydrocarbon chain, as occurs also on Jupiter (see Yung and DeMore, 1999). On modern Titan,
 940 H_2 is scarce, so the "cracking" effect is weak and photochemical cycles involving radical-radical combination lead
 941 to build-up of long chain hydrocarbons which fall out of the atmosphere and form tar like substances on the
 942 surface.

943 Gilliam and McKay (2011) simulated an exo-Titan with the same instellation as modern Titan but placed
 944 around an M4 dwarf star. Results suggested that enhanced incoming IR from the star could penetrate the exo-
 945 atmosphere more efficiently since the haze is more transparent at such wavelengths. This led in their study to
 946 $\sim 10K$ surface warming to $\sim 104K$ which is only $\sim 7K$ below the boiling point of CH_4 . One can therefore imagine
 947 exo-Titans which are moderately warmer than modern Titan so that the methane lakes have evaporated. Finally,
 948 note that proposed cryo-volcanism driven by tidal-heating on modern Titan (see e.g. Tobie et al., 2006) which
 949 could supply CH_4 into Titan's atmosphere from clathrate hydrates beneath the surface - would of course stop
 950 operating had Titan migrated inwards early in its history. This could shorten methane recycling timescales
 951 between surface and atmosphere by removing a potentially significant source.

952 In summary our Titan-based thought experiment suggests that migrated bodies from beyond the ice line
 953 could feature oceans containing ammonia-water mixtures with depressed freezing points or/and atmospheres
 954 consisting of steam-ammonia-methane-nitrogen mixtures depending on e.g. the origin and rate of migration and
 955 the incoming instellation.

957 5.5 Carbon monoxide atmospheres

958 Carbon monoxide (CO) can be formed in planetary atmospheres by several mechanisms including (a) *in-*
 959 *situ* gas-phase processes e.g. via photolysis of CO_2 or (b) outgassing if redox conditions in the mantle are suitable
 960 or (c) *thermodynamically* at high pressures and temperatures. For example, in the middle to lower atmosphere
 961 of Hot Jupiters and sub-Neptunes, CO can be the thermodynamically favored form of carbon for suitable
 962 metallicities.

964 5.5.1 In-situ gas phase formation via CO_2 photolysis

965 CO_2 features temperature-dependent photolysis in the UV absorption band at $120 < \lambda < 210 nm$ to form
 966 $CO(^1\Sigma^+)$ and (mostly) the ground-state $O(^3P)$ triplet together with vibrationally-excited $O(^1D)$ singlet (e.g. Schmidt
 967 et al., 2013). The product $CO(^1\Sigma^+)$ can itself photolyse below 167nm. The atomic oxygen triplet can undergo
 968 three-body (termolecular) self-combination to form O_2 . For Earth-like atmospheres orbiting (F,G,K) stars, Selsis
 969 (2002) suggested that O_2 formed abiotically in CO_2 -dominated atmospheres could limit its own production by
 970 absorbing the same photons needed to split CO_2 . For planets orbiting M-dwarf stars, however, the extended pre-
 971 main sequence and strong early XUV was proposed to drive strong abiotic oxygen production through either (a)
 972 photolysis of CO_2 followed by self-reaction of oxygen or (b) photolysis of H_2O followed by rapid loss of H (see e.g.
 973 Luger and Barnes, 2015) as discussed above. The reverse reaction to the first step in (a) i.e. involving three-body
 974 (termolecular) recombination of CO and O is electronically quantum spin forbidden (Jasper and Dawes, 2013)
 975 and typically proceeds with a gas-phase rate $\sim 10^4$ times slower than the forward photolysis reaction in planetary
 976 atmospheres (Krasnopolsky, 1982).

977 Families of gas-phase reactive species involving e.g. hydrogen oxides (HOx), nitrogen oxides (NOx) and
 978 chlorine oxides (ClOx) can catalytically drive the recombination of CO and O into CO_2 . It is convenient to group
 979 fast-reacting species into "families" in this way since although the individual species can quickly inter-react, the
 980 sum of their concentrations (e.g. $HOx = OH + HO_2$) is removed more slowly from the atmosphere and is therefore
 981 conserved (on timescales of \sim weeks). Calculating the sum HOx, NOx, ClOx etc. is therefore useful since it indicates
 982 the atmosphere's potential to drive catalytic cycles which e.g. form CO_2 from its precursors (on Mars and Venus)
 983 or to destroy ozone (on Earth). The family members are formed from so-called reservoir species which generally
 984 have longer lifetimes (weeks to months) and which typically release the reactive forms, HOx, NOx and ClOx via
 985 photolysis or thermal decomposition. Examples of reservoir molecules include nitric acid (HNO_3), nitrogen
 986 pentoxide (N_2O_5) and hydrochloric acid (HCl).

987 Tian et al. (2014) suggested that high (FUV/NUV) ratios characteristic of M-dwarf stars (with ratio values
 988 up to x100 higher than the Sun) could favor abiotic O_2 from CO_2 photolysis in planetary atmospheres since firstly,
 989 strong FUV favors CO_2 photolysis and secondly, weak NUV favors low release rates of HOx and NOx from their
 990 reservoirs hence weak regeneration of CO_2 . To develop these ideas further, it would be interesting to quantify

991 with climate-chemistry modeling studies the effect of varying (FUV/NUV) upon the release of HOx, NOx and ClOx
 992 in different background atmospheres and to clarify the role(s) of different reservoir molecules over a range of
 993 UV environments considering e.g. weakly-bonded reservoirs such as nitrous acid (HONO) and hypochlorous acid
 994 (HOCl) which photolyse in the visible and NUV respectively; medium-strength reservoirs such as chlorine nitrate
 995 (ClONO₂), peroxyxynitric acid (HO₂NO₂) and nitric acid (HNO₃) which photolyse in the UV and strongly-bound
 996 reservoirs such as HCl and H₂O which photolyse in the UV and EUV. On Mars and Venus, HOx and ClOx cycles
 997 respectively have been suggested to play an important role in regenerating CO₂ (see e.g. Yung and DeMore, 1999
 998 and references therein). Stock et al. (2017) modelled catalytic cycles which operate in the modern Martian
 999 atmosphere. Grenfell et al., (2010) suggested an alternative route to converting CO into CO₂ via heterogeneous
 1000 oxidation of CO on the surface of transition metal containing minerals such as hematite on (hot) planetary
 1001 surfaces.

1002 Could CO-dominated atmospheres build-up in-situ via CO₂ photolysis in the gas-phase? This would
 1003 require firstly, CO₂-rich atmospheres which photolyse into CO plus O under conditions where the reverse reaction
 1004 (reforming CO₂) is suppressed due to a lack of HOx, NOx or ClOx (see Selsis et al., 2002). In general, HOx is formed
 1005 in atmospheres with trace amounts of water vapor in the presence of UV whereas NOx can build up in
 1006 atmospheres containing N₂ with some O₂ in the presence of EUV or/and cosmic rays and lightning. Secondly,
 1007 build-up of a CO-dominated atmosphere would be favored by atmospheres in which the abiotic O₂ formed as a
 1008 by-product of CO₂ photolysis could be removed by weathering (see 5.3 and Zahnle et al., 2008).

1009 In summary, CO atmospheres could therefore be favored for atmospheres with the following conditions:
 1010 (1) strong early CO₂ outgassing, (2) dry atmospheres (suggesting low HOx), (3) weak dynamical transport cells
 1011 (suggesting weak lightning), (4) protected from cosmic rays. Attaining a CO-dominated atmosphere in this way
 1012 would require removal of the co-produced abiotic O₂ via e.g. weathering. More work is required however to
 1013 explore this parameter range. Zahnle et al. (2008) (their Figure 11) explored a parameter range where CO is
 1014 favored depending upon humidity and temperature. They also noted that CO atmospheres on early Mars, if they
 1015 existed, could have left behind metal carbonyls in the Martian soil, which would be a proxy for their existence.

1016 5.5.2 Outgassing

1017 Outgassing of CO directly could also favor formation of CO-dominated atmospheres on early terrestrial
 1018 exoplanets if mantle fugacity is suitable (Miyakawa et al., 2002). On modern Earth, even if carbon were outgassed
 1019 as CO, it would nevertheless be rapidly removed due to its rather short lifetime of ~2 months (Novelli et al., 1994)
 1020 in Earth's damp troposphere which proceeds mainly (~85% Khalil and Rasmussen, 1990) via HOx-catalysed CO-
 1021 oxidation into CO₂ with smaller contributions from surface losses and diffusion into the stratosphere.
 1022

1023 5.5.3 Thermodynamics

1024 Observed values of CO, CH₄ and H₂O in the atmospheres of Hot Jupiters (e.g. Tinetti et al., 2007; de Kok
 1025 et al., 2013) and in particular the [CO/CH₄] ratio have presented a challenge for photochemical-climate-transport
 1026 models to interpret (see e.g. Venot et al., 2014 and references therein). More work for example is required to
 1027 understand better the potential role of e.g. vertical transport, metallicity and photochemistry upon [CO/CH₄] in
 1028 such atmospheres. CO is generally the thermodynamically favored form of carbon compared to CH₄ in (Ultra) Hot
 1029 Jupiters [U(HJs)] for pressure regions typically sampled during emission (Kataria, et al., 2016) such that [CO/CH₄]
 1030 ~10 for cooler HJs increasing to up 10⁻⁸ for UHJs and where the sum [CO+CH₄] constitutes ~1% of the atmosphere.
 1031 More work is required however to understand better the potential role of e.g. vertical transport and
 1032 photochemistry upon the [CO/CH₄] ratio.
 1033

1034 Regarding warm and hot SEs, modeling work by Hu et al. (2014) (their Figures 5 and 6) suggested that
 1035 chemical equilibrium favors CO-dominated atmospheres e.g. for GJ1214b and for 55 Cancri e in the pressure
 1036 region (1-100mb) (assuming 0.5 < X_[C/O] < 2 and X_[H] < 0.5, where 'X' denotes mole fraction) generally observable by
 1037 transmission spectroscopy. More work is required to explore the role of photochemistry and the importance of
 1038 vertical transport which can upwell CO from lower hotter regions where it is thermodynamically favored.
 1039

1040 5.5.4 Other Processes

1041 Additional sources of atmospheric CO potentially important on e.g. Early Earth include delivery of CO
 1042 directly via comets (e.g. Lupu et al., 2007). Another suggested source of CO occurs on the surface of hot metallic
 1043 iron from impact plumes which can reduce CO₂ into CO (Kasting, 1990). Finally, it is interesting to note that
 1044 Miyakawa et al. (2002) suggested there is no geological proxy to *preclude* CO-dominated atmospheres on Early
 1045 Earth and that such atmospheres could even have favored prebiotic synthesis.
 1046

1047 5.6 Sulphur-containing atmospheres

1048 Sulfur and its compounds have fascinatingly diverse applications in planetary science. This diversity
 1049 stems from sulfur's ability to adopt a range of redox and valence states which enable the formation of stable
 1050 chemical compounds applicable to a wide range of chemical and biological systems extending from the planetary
 1051 interior to the lithosphere, hydrosphere and atmosphere.

1052 1053 **5.6.1 Solar System**

1054 Regarding Earth, the modern and ancient global sulfur cycles were reviewed by e.g. Brimblecombe
 1055 (2014) and Fike et al. (2015) respectively. In Earth's core, seismology measurements suggest that light alloying
 1056 elements including sulfur could be present (see e.g. review by Poirier, 1994; sulfur compounds were also
 1057 suggested to occur in the core of other planets such as Mercury (Rivoldini et al., 2009) and Mars (Schubert and
 1058 Spohn, 1990). In Earth's upper mantle, sulfur compounds are estimated to make up 300-400ppm (von Gehlen,
 1059 1992). On Earth's surface sulfur is cycled from lithosphere to interior via burial of oxidized (sulfate) and reduced
 1060 (sulfide) and returned to the atmosphere via outgassing of e.g. H₂S and SO₂. Analyzing deviations from standard
 1061 mass dependent fractionation of isotope ratios in sulfur sediments from the Early Earth (see e.g. Harman et al.,
 1062 2018) can be used as a proxy for atmospheric oxygen abundance.

1063 In modern Earth's atmosphere, important surface sources of sulfur-containing species include: SO₂ (60-
 1064 80 Tg S/yr) and H₂S (7-8 Tg S/yr) arising mainly via anthropogenic and volcanic emissions and dimethyl sulfide
 1065 (DMS) (CH₃-S-CH₃) (13-25 Tg S/yr) arising mainly via biogenic emissions (Sheng et al., 2015). Potentially complex
 1066 gas-phase oxidation cycles in the troposphere (see for example von Glasow and Crutzen, 2004) involving oxidants
 1067 such as hydroxyl (OH) and ozone (O₃) then lead to formation of gas-phase sulfur trioxide (SO₃) which quickly
 1068 undergoes the gas-phase reaction: SO₃+H₂O+M→H₂SO₄+M (where 'M' denotes any species needed to carry away
 1069 excess vibrational energy). The gas-phase products sulfuric acid quickly reacts with liquid water to form sulfate
 1070 aerosol. The so-called Junge layer (Junge et al., 1961) denotes Earth's stable, globally-distributed sulfate aerosol
 1071 peaking around 18-22km which influences climate, clouds and composition. Faloon (2009) review uncertainties
 1072 in the processes affecting atmospheric sulfur in the Earth's marine boundary layer.

1073 On Venus, a thick cloud layer extends from ~48 to 70km which likely consists mostly of sulfate aerosol
 1074 droplets formed from SO₂ oxidation. These clouds strongly influence atmospheric albedo, climate and
 1075 composition. Below the clouds at 35-40km, VEx data (Svedhem et al., 2007) suggested 50-500ppmv SO₂ and 2-8
 1076 ppmv COS. Above the clouds, Mahieux et al. (2015) suggested significant variability of SO₂ (from ~tens to
 1077 hundreds of ppbv) based on Venus Express (VEx) data. Sulfur-based catalytic gas-phase cycles have been
 1078 proposed above the clouds (Yung and Demore, 1999, their chapter 8) to drive recycling of CO back into CO₂ on
 1079 Venus. Recent observations of the glory phenomenon by Vex (Markiewicz et al., 2014) suggested that elemental
 1080 polysulfur chains or/and iron sulfide could be the unknown UV absorber.

1081 On Mars, the presence of mineral sulfates (see e.g. review by King and McLennan, 2010), (which were
 1082 also suggested by the Curiosity Rover, Nachon et al., 2017), together with a general lack of carbonates, suggest
 1083 that sulfur cycles could have played an important role in the lithosphere-atmosphere system on early Mars. Some
 1084 works e.g. Tian et al., (2009), Kerber et al., (2015) modelled the influence of atmospheric SO₂ and sulfate aerosol
 1085 upon climate on early Mars. Results suggested e.g. that sulfate aerosol cooling could prevent SO₂ greenhouse
 1086 heating from producing habitable surface conditions. Halevy and Head (2014) used an updated model to
 1087 reinvestigate this problem. They found that on a cold, early, dusty Mars the net effect of SO₂ outgassing could
 1088 be warming yet could be cooling if the atmosphere is clear, consistent with the findings in Tian et al. (2009).

1089 In the outer Solar System, observations of sulfur-containing atmospheric species are rather sparse.
 1090 Wong et al. (2004) suggested (68-110) ppmv of H₂S in the deep Jovian atmosphere (from 8.9-11.7 bar) based on
 1091 a revised Galileo Probe analysis. Sulfur-containing species could make up an important constituent of clouds e.g.
 1092 NH₄SH detected on Saturn (Baines et al., 2009) and H₂S on Uranus (Irwin et al., 2018). Regarding the icy moons,
 1093 SO₂ has been detected on Io as discussed above (see Table 1). Moses et al. (2002) modelled photochemical
 1094 responses of sulfur species during volcanic eruptions on Io. Some studies hypothesized biogeochemical cycles
 1095 including sulfate occurring in the deep oceans of icy moons such as Europa (Zolotov and Shock, 2004).

1096 Regarding exoplanets, what range of sulfur-containing atmospheres could be feasible? On terrestrial
 1097 planets under oxidizing conditions (e.g. on Earth or above the cloud-top on Venus) in the presence of UV, reduced
 1098 sulfur compounds could form oxidized species such as SO₃. This species quickly reacts with trace amounts of
 1099 water vapor to form sulfate aerosol. Under reducing conditions (e.g. on giant planets), on the other hand,
 1100 reduced sulfur species such as NH₄SH or/and elemental sulfur could condense to form aerosol. The model study
 1101 by Hu et al. (2013) for example, who investigated H₂-dominated atmospheres for SEs for example suggested the
 1102 presence of sulfur which can form multiple structures including a stable S₈ crown (whose spatial arrangement
 1103 leads to low strain on the S-S bonding) which could condense and form aerosol. Kaltenecker and Sasselov (2010)
 1104 discuss spectral signals for sulfur species assuming hypothetical exoplanetary geochemical sulfur cycles.
 1105 Regarding gas planets, Zahnle et al., (2016) also noted the potential importance of S₈ hazes in their model study

1106 of the warm Jupiter 51 Eri b. Zahnle et al. (2009) discussed sulfur photochemistry on hot Jupiters (see also Gao
 1107 et al., 2015). Loftus et al. (2019) evaluated the co-existence of a thick (observable) sulphur aerosol haze layer
 1108 together with a significant ocean on a rocky exoplanet, including the fundamentals of the sulphur cycle. Results
 1109 suggest that such an observable haze layer is not compatible with such an ocean.

1110 Could sulfur containing or even sulfur-dominated atmospheres be common in nature? There are
 1111 theoretical arguments which suggest that the build-up sulfur-dominated atmospheres could be challenging: in
 1112 oxidizing atmospheres, sulfur species would be converted to sulfate aerosol which would eventually undergo
 1113 removal via deposition or washout; in reducing atmospheres e.g. elemental sulfur such as stable S₈ could similarly
 1114 build-up, condense and undergo removal. The extent by which sulfur species can build up depends therefore on
 1115 the UV intensity and the abundance of water-vapor. Increased sulfur abundances are expected to be favored for
 1116 weak UV, dry conditions.

1117

1118 5.7 Nitrogen Atmospheres

1119 Nitrogen species play a major role in planetary atmospheres, influencing climate, composition and (on
 1120 Earth) biogeochemical cycling. Modern VEM have surface partial pressures of N₂ equal to (3.3, 0.78 and 1.7x10⁻⁴)
 1121 bar respectively (Yung and DeMore, 1999). VEM interiors are estimated to have (2.2, 3.4, 0.3) (in units of 10¹⁹)
 1122 kg N respectively (Johnson and Goldblatt, 2015) where values are uncertain by a factor of two to three. The
 1123 evolution of atmospheric nitrogen on VEM and terrestrial exoplanets was discussed e.g. in Lammer et al., (2019).
 1124 Wordsworth (2016) suggested that enhanced nitrogen in the Venusian atmosphere compared with Earth could
 1125 be related to stronger N₂ outgassing on Venus, related to enhanced oxidation of the mantle due to enhanced
 1126 H₂O photolysis followed by H-escape. Goldblatt et al. (2009) and Wordsworth and Pierrehumbert (2013)
 1127 suggested that atmospheric molecular nitrogen could have helped warm the early Earth to achieve and maintain
 1128 habitable conditions. A difficulty of this hypothesis is that the atmospheric pressure on Archean Earth might have
 1129 been too low to support a strong N₂-H₂ greenhouse effect based on measured raindrop distributions ~3 Ga (Som
 1130 et al., 2012; Som et al., 2016). The model study of von Paris et al. (2013) suggested that adding 0.5 bar N₂ to the
 1131 early Martian atmosphere led to +13K surface warming. In the present work, we summarize important general
 1132 processes affecting atmospheric nitrogen evolution with the aim of discussing what possible range of
 1133 atmospheric N₂ abundances could be expected on terrestrial exoplanets. We do not focus here on the so-called
 1134 waterworlds since potential nitrogen cycles on such worlds are likely very different (see discussion in Lammer et
 1135 al., 2019).

1136 Important processes affecting planetary nitrogen evolution include (1) *delivery* during planet formation
 1137 via nitrogen-containing ices present on bodies from the outer solar system (see section 3.4.4). Recent estimates
 1138 of modern Earth's nitrogen budget suggest ~x50 times the present day Atmospheric Mass N₂ (AMN) which is
 1139 mainly stored in the mantle (~x7 AMN in reduced forms, NHx) and possibly a large reservoir in the core (~x43
 1140 AMN alloyed with iron in the form Fe_xN_y as suggested by Laneuville et al., 2018, their Table 1) (see also Marty,
 1141 1995); (2) regarding early hydrodynamic *escape* of nitrogen, Lammer et al., (2018) discussed weak loss on early
 1142 Venus and Earth but efficient loss on early Mars based on nitrogen isotope data; (3) *outgassing* which depends
 1143 on mantle redox and pH which determine whether nitrogen exists in the molecular state (easily outgassed,
 1144 favored at pH ~1-3 at ~positive Quartz-Fayalite-Magnetite buffer values in mantle wedges) or in the ammoniac
 1145 (NH₄⁺) state (easily retained, favored at negative pH in the upper mantle, see e.g. Mikhail et al., (2017) and Zerkle
 1146 and Mikhail (2017) their Figure 2). Lammer et al., (2019) suggested ambient N₂ reached up to ~0.2bar during the
 1147 Archaean associated with e.g. outgassing at the magma ocean phase; (4) efficient *dissolution* of outgassed N₂
 1148 into the mantle during the MO phase (Wordsworth, 2016); (5) efficient biological *fixation* and *denitrification* with
 1149 a rate of ~1-2 x10² Tg N year on modern Earth (Laneuville et al., 2018; see also Canfield, 2010); (6) *lightning* which
 1150 fixates molecular nitrogen at a rate of ~(3-10)x10⁹kg N/yr on modern Earth (Laneuville et al., 2018). The resulting
 1151 nitrogen-containing reactive species form nitrogen oxides or/and nitric acid (HNO₃) which is efficiently dissolved
 1152 by scavenging rain droplets and washed out into the ocean on timescales of weeks to months to form
 1153 thermodynamically stable nitrate (NO₃⁻) anions; (7) *cosmic rays* (see discussion below) which can remove N₂ and
 1154 O₂ on Earth especially at higher latitudes during strong solar activity (see e.g. Jackman et al., 2005); molecular
 1155 nitrogen can be returned to the atmosphere via outgassing with an estimated rate (including the contribution
 1156 from mid-ocean ridges) of up to ~0.4x10⁹ kg N/yr (Laneuville et al., 2018, their section 2.6); (8) meteoritic impacts
 1157 can thermolyse atmospheric nitrogen where reaction products form nitrogen oxides and are removed from the
 1158 atmosphere (Grady et al., 1998); (9) *escape*, depending upon upper atmosphere temperature and incoming XUV
 1159 on the Hadean Earth which are not well constrained (see discussion in e.g. Lammer et al., 2019).

1160 Regarding theories and proxy data for nitrogen on early Earth, surface partial pressure of nitrogen was
 1161 likely low during Earth's magma ocean phase due to efficient dissolution of nitrogen from the atmosphere into
 1162 the hot mantle (see Lammer et al., 2019; Wordsworth, 2016). Som et al. (2012) suggested an upper limit of about
 1163 twice modern levels for Archaean surface air density based on an analysis of fossilized raindrop imprints.

1164 Kavanagh and Goldblatt (2015) revised the method and suggested an upper limit of about four times the modern
1165 value. An updated study by Som et al. (2016) then revised downwards the Archean upper limit for atmospheric
1166 surface density, to a value less than half the modern amount. Regarding model studies, Rimmer and Rugheimer
1167 (2019) suggested that ~ 0.3 bar surface pressure on Early Earth would enable sufficient oxidizing conditions in the
1168 upper atmosphere to oxidize incoming Archaean micrometeorites, consistent with proxy data. Johnson and
1169 Goldblatt (2018) modelled the biogeochemical nitrogen cycle including deep and shallow ocean
1170 parameterizations and linking with phosphorous chemistry in the lithosphere. Their results for surface nitrogen
1171 partial pressure over Earth's history varied from about (0.1 to 6.0) times the present day atmospheric nitrogen
1172 level, depending upon uncertainties in the amount of nitrogen in the bulk silicate Earth (BSE) as well as the timing
1173 and magnitude of key processes such as burial, continental evolution, weathering and biological activity. In order
1174 for their evolutionary scenarios to finish with the correct present day atmospheric nitrogen (PAN) required (4 to
1175 6) times PAN to be present in the BSE. Stüeken et al. (2016) applied an Earth system box model to study the
1176 evolution of nitrogen on Earth. Results suggested that depending on uncertainties in nitrogen burial rates (which
1177 can strongly fluctuate based on the geological record) the surface partial pressure of nitrogen can vary from
1178 about (0.1 to 1.1) times the present day value.

1179 Regarding exoplanets, Lammer et al. (2019) considered the effect upon atmospheric nitrogen evolution
1180 for (a) an Earth-like planet without plate tectonics, (b) a planet with anoxic life, and (c) an Earth-like planet where
1181 life becomes extinct. Their results suggested that in case (a) the absence of plate tectonics would hinder mixing
1182 of oxidized forms of nitrogen into the mantle. This suggests enhanced abundances of nitrogen in its reduced
1183 forms (e.g. NH_4^+) in the interior, which are more easily retained hence only a weak conversion to N_2 and reduced
1184 outgassing of nitrogen. In case (b) anoxic fixation in the absence of denitrification led to low atmospheric nitrogen
1185 whereas in case (c) the absence of nitrogen recycling associated with life resulted in atmospheric nitrogen
1186 removal via lightning and cosmic rays leading to low atmospheric abundances. Stüeken et al. (2016) also applied
1187 a biogeochemical box model to scenarios of anoxic planets with and without life. Their results suggested that
1188 whether atmospheric nitrogen could recover to present day levels depended on the rate of burial assumed and
1189 whether or not continents were assumed to be present (scenarios without continents did not lead to nitrogen
1190 recovery). Laneuville et al. (2018) modeled atmospheric nitrogen evolution on an Earth-like planet without life
1191 and suggested variations from $\sim(0.2$ to 8) times the present atmospheric level (PAL) depending mainly on
1192 uncertainties in the atmospheric fixation rate due to e.g. lightning and cosmic rays, with a weaker variation of
1193 $\sim(0.6$ to 2) PAL arising due to uncertainties in mantle mixing and ocean circulation.

1194 Regarding Earth-like planets orbiting in the close-in HZ of active, low mass stars, the atmosphere could
1195 be strongly exposed to high energy particles (Grenfell et al., 2012; Tabataba-Vakili et al., 2016; Scheucher et al.,
1196 2018; Herbst et al., 2019, see also Airapetian et al., 2018). Stellar proton events (SPEs) on Earth can dissociate
1197 molecular nitrogen and lead to $\sim 2 \times 10^{33}$ NO molecules/day (Jackman et al., 2005, their Table 1). Assuming such
1198 events are experienced continuously for an Earth-like planet orbiting an active M-dwarf star, would lead to a
1199 removal rate of atmospheric nitrogen due to cosmic rays of 0.04 Tg NO/yr. By comparison, lightning fixation on
1200 modern Earth (which without life would remove atmospheric nitrogen within a few hundred Myr without
1201 regassing; Laneuville et al., 2018) removes atmospheric nitrogen about x100 slower. For superflaring stars
1202 however (see e.g. Davenport, 2016) the cosmic ray fluxes could be 10^3 to 10^5 times higher than Earth SPEs,
1203 suggesting nitrogen removal fluxes up to ~ 4000 Tg/yr which would remove Earth's atmospheric nitrogen in $\sim 10^5$
1204 years. In addition to potentially strong nitrogen removal due to cosmic rays, lightning removal could also be
1205 potentially strong on, for example, tidally-locked Earth-like exoplanets which could have strong day to night
1206 transport cells, although such effects are not well quantified. Planets with high meteoritic bombardment could
1207 fix and efficiently remove atmospheric nitrogen.

1208 In summary, what range of N_2 atmospheres could we expect in terrestrial exoplanets? Earth system
1209 modeling suggests values from below a tenth of a bar up to several bar over Earth's history. Isotope estimates
1210 suggest a large range up to ~ 43 times the present day atmospheric budget in the Earth's core. The extent and
1211 rate at which nitrogen is removed to the core during planet formation needs further study. The main
1212 uncertainties in atmospheric processes lie in the distribution of nitrogen in the Earth system and the timing and
1213 nature of key processes such as biology and subduction. Model feedbacks such as the effect of e.g. atmospheric
1214 oxidation via escape and the influence upon the interior are lacking. A detailed intercomparison of current
1215 nitrogen cycle models including their reservoirs and fluxes for clearly defined scenarios would be informative.
1216 On a positive note, there is some hope that exoplanet science could help by constraining nitrogen abundances
1217 from observing spectroscopic collisional pairs (Schwieterman et al., 2015 as mentioned above) which will be
1218 invaluable in disentangling the possible evolution scenarios.

1219
1220
1221

6. Conclusions

- 1222
- 1223
- 1224
- 1225
- 1226
- 1227
- 1228
- 1229
- 1230
- 1231
- 1232
- 1233
- 1234
- 1235
- 1236
- 1237
- 1238
- 1239
- 1240
- 1241
- 1242
- 1243
- 1244
- 1245
- 1246
- 1247
- 1248
- 1249
- 1250
- 1251
- 1252
- 1253
- Key properties such as the metallicity and early rotation rates of interstellar clouds could vary systematically across the Galaxy. The extent by which this variation could imprint itself upon resulting planetary diversity is currently unclear.
 - Although tenuous atmospheres could have weak spectral features they could nevertheless feature large “cometary like” tails and transmission windows down to the surface - making them favorable targets in this respect.
 - If water delivery to rocky exoplanets depends mainly on impact-induced de-volatization during formation then water-rich terrestrial worlds could be quite common. If however it depends on a “Grand Tack” type analogue then more work is required to investigate how this mechanism operates for different exoplanetary systems.
 - Magma oceans with silicate atmospheres, light primordial atmospheres and outgassing of massive steam atmospheres could be universal stages in the evolutionary track of rocky worlds. How long these phases endure however depends on key processes such as instellation, escape and outgassing.
 - The relative occurrence of oxidized atmospheres (e.g. O₂, CO₂, CO, H₂O) compared with reduced atmospheres (CH₄ and higher hydrocarbons) and other atmospheric compositions (e.g. sulfur and nitrogen-containing species) depends on numerous processes such as the initial disk metallicity and its dynamics, how efficiently the planetary interior stores reduced compounds and also upon long-term escape, outgassing and biogeochemical cycling.
 - Sulfur species can form aerosols in both oxidized and reduced atmospheres. Build-up of such aerosols would eventually be limited by sedimentation and surface deposition. Sulfur-rich atmospheres could be favored where conditions are (a) dry, since water is needed to form sulfate from its precursors, or (b) have weak UV, which leads to suppressed formation of aerosol precursors.
 - Nitrogen abundances in the atmosphere vary over two orders of magnitude depending upon uncertainties in interior, subduction and biological processes.

1254 **Acknowledgements**

1255 This project has received funding from the European Research Council (ERC)
 1256 under the European Union’s Horizon 2020 research and innovation program (grant agreement No.
 1257 679030/WHIPLASH). This project is partly supported by the International Space Science Institute (ISSI)
 1258 in the framework of an international team entitled “Understanding the Diversity of Planetary Atmospheres.”
 1259 This project has received funding from the European Union’s Horizon 2020 research and innovation program
 1260 under the Marie Skłodowska-Curie Grant Agreement no. 832738/ESCAPE. M.T. acknowledges funding
 1261 from the Gruber Foundation. This work has been carried out within the framework of the NCCR PlanetS
 1262 supported by the Swiss National Science Foundation. This research has made use of NASA’s Astrophysics
 1263 Data System. LN and JLG acknowledge support from the Deutsche Forschungsgemeinschaft (DFG, German
 1264 Research Foundation) Project ID 263649064 TRR 170. This is TRR 170 Publication No. 87. The authors
 1265 thank ISSI Teams 370 and 464 for fruitful discussions. Mareike Godolt acknowledges support by the German
 1266 science foundation through project GO 2610/1-1 and the priority program SPP 1992 “Exploring the Diversity
 1267 of Extrasolar Planets” (GO 2610/2-1).

1268

1269 **References**

- 1270 Abe, Y., Earth Moon Plan., 108, 9-14 (2011)
- 1271 Adibekyan, V., et al., A&A, 581, L2 (2015)
- 1272 Airapetian, V. S., et al., ApJL, 863, 1 (2017)
- 1273 Airapetian, V. S., et al., Nat. Ast., 2, 448 (2018)
- 1274 Alibert, J., and Venturini, J., A&A, 626, A21 (2019)
- 1275 Ali-Dib, M., et al., ApJ, 793, 1 (2014)

- 1276 Allart, R., et al., *Science*, 362, 1384-1387 (2018)
- 1277 Angelo, I., and Hu, R, *Astrophys. J.* 154, 232 (2017)
- 1278 Anglada-Escudé et al., *Nature*, 536, 437-440 (2016)
- 1279 Armstrong, K., et al., *Science*, 365, 903-906 (2019)
- 1280 Atreya, S., et al., *PSS*, 47, 1243-1262 (1999)
- 1281 Atreya, S., et al., *Space Sci. Rev.*, 216, 18, 1-31 (2020)
- 1282 Bagenal, F., et al., "Jupiter, the planet, satellites and magnetosphere", *Camb. Uni. Press* (2004)
- 1283 Baines, K. H., et al., *PSS*, 57, 1650-1658 (2009)
- 1284 Batalha, N. M., et al., 2011, *ApJ*, 729, 1-21 (2011)
- 1285 Baumeister, P., et al., *ApJ*, 889, 1-42 (2020)
- 1286 Benneke, B., et al., *Nature Astron.*, 3, 813-821 (2019)
- 1287 Berner, R. A., *Geochim. Cosmochim. Acta*, 65, 685-694 (2001)
- 1288 Bétrémiux, J., and Kaltenegger, L., *ApJ*, 791, 7, 1-12 (2014)
- 1289 Bolmont, E., et al., *MNRAS*, 464, 3728-3741 (2017)
- 1290 Booth, R. A., *MNRAS*, 469, 3994-4011 (2017)
- 1291 Booth, R. A. and Ilee, J. D., *MNRAS*, 487, 3998-4011 (2019)
- 1292 Boro Sakia, S., et al., *A&A*, 635, A178 (2020)
- 1293 Boukaré, C.-E., et al., *Earth Plan. Sci. Lett.*, 491, 216-225 (2018)
- 1294 Bourrier, V., et al., *A&A*, 599, L3 (2017)
- 1295 Bourrier, V., et al., *A&A*, 619, 1 (2018)
- 1296 Brimblecombe, P., *Treat. Geochem.* (2nd edition), 10, 559-591 (2014)
- 1297 Budaj, J., *A&A*, 557, A72 (2013)
- 1298 Burke, C. J., et al., *ApJ*, 809, 1 (2015)
- 1299 Canfield, D. E., et al., *Science*, 330, 192-196 (2010)
- 1300 Carlson, R. W., *Science*, 283, 820 (1999)
- 1301 Catling, D. C., and Claire, M. W., *Earth Planet. Sci. Lett.*, 237, 1-20 (2005)
- 1302 Catling, D. C., et al., *Science*, 293, 839-843 (2001)
- 1303 Cauley, P. W., et al., *Nature Astron.*, 3, 1128-1134 (2019)
- 1304 Ceppi, and Hartmann, *Curr. Clim. Change Rep.*, 1, 94-102 (2015)
- 1305 Charnay, B., et al., *ApJL*, 813, 1 (2015)
- 1306 Charnay, B., et al., Chapter 3, in "Understanding the Diversity of Planetary Atmospheres" (ed. Forget, F., et al.), *Spa. Sci. Rev.* (in preparation) (2020)
- 1308 Cassata, S., *Earth Plan. Sci. Lett.*, 479, 322-329 (2017)
- 1309 Chaisson, E., and McMillan, S., *Astron. today*, 3rd edition, Prentice-Hall (1999)
- 1310 Chen, G., et al., *A&A*, 635, A171 (2020)
- 1311 Coustenis, A., et al., *A&A*, 9, 249-268 (2009)
- 1312 Cui, W., et al., *Earth Plan. Phys.*, 2, 247-256, (2018)
- 1313 Dasgupta, R., *Rev. Min. Geochem.*, 75, 183-229 (2013)
- 1314 Davenport, J. R. A., *ApJ*, 829, 23 (2016)
- 1315 Dehant, V., et al., *Spa. Sci., Rev.*, 215, 42, 1-48 (2019)
- 1316 Demory, B. O., et al., *A&A*, 533, A114 (2011)
- 1317 Demory, B. O., et al., *MNRAS*, 455, 2018-2027 (2016^a)
- 1318 Demory, B. O., et al., *Nature*, 532, 207-209 (2016^b)
- 1319 De Kok, B. J., et al., *A&A*, 554, A82, (2013)
- 1320 De Wit, J., et al. *Nazire Astron.*, 2, 214-219 (2018)
- 1321 Dorn, C., et al., *A&A*, 577, A83 (2015)
- 1322 Dorn, C., et al., *A&A*, 597, A37 (2017)
- 1323 Dorn, C., and Heng, K., *ApJ*, 853, 1 (2018)
- 1324 Dong, C., et al., *PNAS*, 115, 2 (2018)
- 1325 Dorn, C., et al., *MNRAS*, 484, 712-727 (2019)
- 1326 Douglas, E. S., et al., *Proc. SPIE* 10705 (2018)
- 1327 Dyudina, U. A., et al., *Science*, 319, 1801 (2008)
- 1328 Ehrenreich, D., et al., 522, 459-461 (2015)
- 1329 Elkins-Tanton, L. T., et al., *Earth Plan. Sci. Lett.*, 271, 181-191 (2008)
- 1330 Elkins-Tanton, L. T., *Astrophys. Spa. Sci.*, 332, 359-364 (2011)
- 1331 Elkins-Tanton, L. T., et al., *Ann. Rev. Earth Plan. Sci.*, 40, 113-139 (2012)
- 1332 Erkaev, N. V., et al., *MNRAS*, 460, 1300-1309 (2016)
- 1333 Esteves, L. J., et al., *APJ*, 804, 1-28 (2015)

- 1334 Farihi, J., *New Astron. Rev.*, 71, 9-34 (2016)
- 1335 Farooqa, I., *Atm. Env.*, 43, 2841-2854 (2009)
- 1336 Fauchez, T. J., et al., *Nature Astron.*, 4, 372-376 (2020)
- 1337 Fegley, B., and Schaefer, L. K., *Treatise on Geochem.*, Chapter 13.3, (2012)
- 1338 Fegley, B., et al., *ApJ*, 823, 103 (2016)
- 1339 Fike, D. A., et al., *Ann. Rev. Earth Plan. Sci.*, 43, 593-622 (2015)
- 1340 Fischer, W. W., et al., *Ann. Rev. Earth Plan. Sci.*, 44, 647-683 (2016)
- 1341 Fischer-Gödde, M., and Kleine, T., *Nature*, 541, 525-527 (2017)
- 1342 Flasar, F. M., et al., *Nature*, 427, 132-135 (2004)
- 1343 Foley, B. J., and Smye, A. J., *Astrobiol.*, 18, 873-896 (2018)
- 1344 Folsom, C. P., et al., *A&A*, 633, A48, (2020)
- 1345 Fontenla, J. M., et al., *ApJ*, 830, 2 (2016)
- 1346 Forget, F., and Leconte, J., *Phil. Trans. Roy. Soc. A*, A372:20130084 (2014)
- 1347 Fratanduono, D. E., et al., *Phys. Rev. B.*, 97, 214105 (2018)
- 1348 Frost, D. J., and McCammon, C. A., *Ann. Rev. Earth Plan. Sci.*, C. A., 36, 389-420 (2008)
- 1349 Fulton, B. J., et al., *AJ* 154, 3 (2017)
- 1350 Fulton, B. J. and Petigura, E., *AJ*, 156, 6 (2018)
- 1351 Frustagli, G., et al., *A&A*, 633, A133 (2020)
- 1352 Füre, E., and Marty, B., *Nature Geosci.*, 8, 515-522 (2015)
- 1353 Furuya et al., *ApJ* 779, 1 (2013)
- 1354 Gaillard, F., and Scaillet, B., *Earth Plan. Sci. Lett.*, 403, 307-316 (2014)
- 1355 Gaillard, F., Scaillet, B., Pichavant, M., Iacono-Marziano, G., *Chem. Geol.* 418, 217–233 (2015)
- 1356 Gaillard, F., et al., Chapter 2, in “Understanding the Diversity of Planetary Atmospheres” (ed. Forget, F., et al.), *Spa. Sci. Rev.* (in preparation) (2020)
- 1357 Gale, J., and Wandel, A., *Int. J. Astrobiol.*, 16, 1-9 (2017)
- 1358 Gans, B., et al., *Phys. Chem. Chem. Phys.*, 13, 8140-8152 (2011)
- 1359 Gao, P., and Benneke, B., *ApJ*, 863, 165 (2018)
- 1360 Gao, P., et al., *ApJ*, 806, 2, 1-12 (2015)
- 1361 García Muñoz, A., et al., *ApJ*, 755, 103 (2012)
- 1362 Gebauer, S., et al., *Astrobiol.*, 17, 27-54 (2017)
- 1363 Gebauer, S., et al., *Astrobiol.*, 18, 856-872 (2018)
- 1364 Von Gehlen, K., *Early Organic Evolution* (Springer, Berlin) (1992)
- 1365 Gilliam, A. E., and McKay, C. P., *PSS*, 59, 835-839 (2011)
- 1366 Gillon, M., et al., 452, 456-460 (2017)
- 1367 Gladstone, G. R., et al., *Science*, 351, 6279 (2016)
- 1368 Von Glasow, R., and Crutzen, P. J., *Atm. Chem. Phys.*, 4, 589-608 (2004)
- 1369 Godolt, M., et al., *A&A*, 592, A36 (2016)
- 1370 Godolt, M., et al., *A&A*, 625, A12, 1-15 (2019)
- 1371 Goldblatt, C., et al., *Nat. Geosci.*, 2, 891-896 (2009)
- 1372 Goldblatt, C., *Astrobiol.*, 15, 362-370 (2015)
- 1373 Grady, M. M., et al., *Geol. Soc.*, 140, 1-5 (1998)
- 1374 Greene, T. P., et al., *ApJ*, 817, 17, 1-22 (2016)
- 1375 Grenfell, J. L., *Landolt-Börnstein Encyclopedia, Astronomy and Astrophysics*, ed. Trümper, J. E., Springer Verlag Berlin Heidelberg, Chapter 4.2.3.6 „Atmospheres of the Planets and Satellites“ (2009)
- 1376 Grenfell, J. L., et al., *PSS*, 58, 1252-1257 (2010)
- 1377 Grenfell, J. L., et al., *Astrobiol.*, 12, 1109-1122 (2012)
- 1378 Grenfell, J. L., et al., *ApJ*, 861, 1 (2018)
- 1379 Grenfell, J. L., et al., *Exp. Astron.*, accepted (2020)
- 1380 Grevesse, N., et al., *Spa. Sci. Rev.*, 130, 105-114 (2007)
- 1381 Grewal, D. S., et al., *Sci. Adv.*, 5, 1, eaau3669 (2019)
- 1382 Guenther, E. W., et al., *A&A*, 525, A24 (2011)
- 1383 Guenther, E. W., and Kislyakova, K. G., *MNRAS*, 491, 3974-3982 (2020)
- 1384 Guillot, T., *Science*, 286, 72-77 (1999)
- 1385 Gumsley, A. P., et al., *PNAS*, 114, 1811-1816 (2017)
- 1386 Gupta, M., and Schlichting, H. E., *MNRAS*, 487, 24-33 (2019)
- 1387 Halevy, I., and Head, J. W., *Nature Geo.*, 7, 865-868 (2014)
- 1388 Hall, D. T., et al., *Nature*, 373, 667 (1995)
- 1389 Hall, D. T., et al., *ApJ*, 499, 475 (1998)

- 1392 Hamano, K., et al., *Nature*, 497, 607-610 (2013))
- 1393 Hammond, M., and Pierrehumbert, R. T., *ApJ*, 849, 152 (2017)
- 1394 Harman, C. E., et al., *Earth Plan. Sci. Lett.*, 496, 238-247 (2018)
- 1395 Hartnett, H. E., et al., *Nature*, 391, 572-575 (1998)
- 1396 Hawker, G. A., and Parry, I. R., *MNRAS*, 484, 4855-4864 (2019)
- 1397 Hayden, M. R., et al., *ApJ*, 808, 132, 1-18 (2015)
- 1398 Hellard, H., et al., *ApJ*, 889, 1-66 (2020)
- 1399 Henning, W. G., et al., White Paper (Pages 1-6) submitted to the National Academy of Sciences Exoplanet Science Strategy Call (2018)
- 1400
- 1401 Herbort, O., et al., *A&A*, accepted (2020)
- 1402 Herbst, K., et al., *A&A*, 631, A101, (2019)
- 1403 Hemingway, D., et al., *Nature*, 500, 550-552 (2013)
- 1404 Holland, H. D., *Cosmo. Chim. Acta*, 66, 3811-3826 (2002)
- 1405 Holland, H. D., *Phil. Trans. Roy. Soc.*, 361, 470 (2006)
- 1406 Hin, R. C., et al., *Nature*, 549, 511-515 (2017)
- 1407 Hirschmann, M. M., *Earth Plan. Sci. Lett.*, 341-344, 48-57 (2012)
- 1408 Hoey, W. A., et al., *Icarus*, 287, 87-102 (2017)
- 1409 Hu, R., et al., *ApJ*, 752, 1, 1-15 (2012)
- 1410 Hu, R., et al., *ApJ*, 769, 6, 1-14 (2013)
- 1411 Hu, R., and Seager, S., *ApJ*, 784, 1 (2014)
- 1412 Hu, R., et al., *ApJ*, 807, 8, 1-14 (2015)
- 1413 Hutsemékers, D., et al., *Icarus*, 204, 346-348 (2009)
- 1414 Irwin, P. J. G., et al., *Nature Astron.*, 2, 420-427 (2018)
- 1415 Jackman, C. H., et al., *Adv. Spa. Res.*, 35, 445-450 (2005)
- 1416 Jacobson, S. A., and Morbidelli, A., *Phil. Trans. Roy. Soc. A*, 372, 1-25 (2014)
- 1417 Jakosky, B. M., et al., *Icarus*, 315, 146-157 (2018)
- 1418 Jasper, A. W., and Dawes, R., *J. Chem. Phys.* 139, 154313, 1-13 (2013)
- 1419 Jin, S., and Mordasini, C., *ApJ*, 853, 2 (2018)
- 1420 Johnson, B., and Goldblatt, C., *Earth Sci. Rev.*, 148, 150-173 (2015)
- 1421 Johnson, B., and Goldblatt, C., *Geochem. Geophys. Geosys.*, 19, 2516-2542 (2018)
- 1422 Johnstone, C. P., et al., *ApJL*, 815, L12 (2015)
- 1423 Johnstone, C. P., et al., *A&A*, 617, A107 (2018)
- 1424 Johnstone, C. P., et al., *A&A Lett.*, 624, L10 (2019)
- 1425 Jontoff-Hutter, D., *Ann. Rev. Earth Okan. Sci.*, 47, 141-171 (2019)
- 1426 Junge, C. E., et al., *Science*, 133, 3463 (1961)
- 1427 Kadoya, S., *Geochem. Pers. Lett.*, 13, 25-29 (2020)
- 1428 Kaltenecker, L., and Sasselov, D., *ApJ*, 708, 2, 1162-1167 (2010)
- 1429 Kasting, J. F., *Orig. Life and Evol. Bios.*, 20, 199-231 (1990)
- 1430 Kasting, J. F., et al., *J. Geol.*, 101, 2 (1993)
- 1431 Kataria, T., et al., *ApJ*, 821, 1-16 (2016)
- 1432 Kavanagh, L., and Goldblatt, C., *Earth Plan. Sci.*, 413, 51-58 (2015)
- 1433 Kawashima, Y. et al., *ApJL*, 876 1 (2019)
- 1434 Katyal, N., et al., *ApJ*, 875, 31, 1-18 (2019)
- 1435 Kerber, L., et al., *Icarus*, 261, 133-148, (2015)
- 1436 Khalil, M. A. K., and Rasmussen, R. A., *Chemosphere*, 20, 227-242 (1990)
- 1437 Kiang, N., et al., *Astrobiol.*, 7, 252-274 (2007)
- 1438 King, P. L., and McLennan, S. M., *Elements*, 6, 107-112 (2010)
- 1439 Kislyakova, K. G., et al., *Astrophys. Spa. Sci. Lib.*, Springer, 441, 137-151 (2015)
- 1440 Kite, E. S., et al., *ApJ*, 828, 80 (2016)
- 1441 Kite, E. S., and Ford, E. B., *ApJ*, 864, 1 (2018)
- 1442 Kite, E. S., *Spa. Sci. Rev.*, 215, 10 (2019)
- 1443 Komacek, T. D. and Showman, A. P.: *ApJ* **821**, 16 (2016)
- 1444 Korablev, O., et al., Chapter 14, in "Understanding the Diversity of Planetary Atmospheres" (ed. Forget, F., et al.), *Spa. Sci. Rev.* (in preparation) (2019)
- 1445
- 1446 Kopparapu, R. K., et al., *ApJ*, 765, 2 (2013)
- 1447 Koskinen, T. T., and Guerlet, S., *Icarus*, 307, 161-171, (2018)
- 1448 Krasnopolsky, V. A., *Photochemistry of the atmospheres of Venus and Mars*, Springer Verlag (1982)

- 1449 Krasnopolsky, V. A., Spectroscopy of planetary atmospheres and ionospheres, Chapter 13: Titan, Cambridge
1450 University Press, (2019)
- 1451 Kreidberg, L., et al., *Nature*, 505, 69-72 (2014)
- 1452 Krivov, A. V., and Booth, M., *MNRAS*, 479, 3300-3307 (2018)
- 1453 Krissansen-Totton, J., et al., *Astrobiol.*, 16, 39-67 (2016)
- 1454 Krissansen-Totton, J., et al., *Sci. Adv*, 4, 1-13 (2018)
- 1455 Kubyshkina, D., et al., *ApJL*, 866, L18 (2018)
- 1456 Kulow, J. R., et al., *ApJ*, 786, 132 (2014)
- 1457 Kurokawa, H., and Kaltenecker, L., *MNRAS* 433, 3239-3245 (2013)
- 1458 Lammer, H., et al., *MNRAS*, 430, 1247-1256 (2013)
- 1459 Lammer, H., et al., *Astron. Astrophys. Rev.*, 26, 2, 1-72 (2018)
- 1460 Lammer, H., et al., *Astrobiol.*, 19, 927-950 (2019)
- 1461 Laneuville, M., et al., *Astrobiol.*, 18, 897-914 (2018)
- 1462 Lammer, H., et al., *Icarus*, 339 (in press) (2020)
- 1463 Lasaga, A. C., and Ohmoto, H., *Geochem. Cosmochim. Acta*, 66, 361-381, (2002)
- 1464 Laughlin, G., Mass-Radius Relations of Giant Planets: The Radius Anomaly and Interior Models. In: Deeg H.,
1465 Belmonte J. (eds) *Handbook of Exoplanets*. Springer, Cham (2018)
- 1466 Lebonnois, S., et al., *Icarus*, 218, 707-722 (2012)
- 1467 Lebrun, T., et al., *J. Geophys. Res.*, E118, 1155-1176 (2013)
- 1468 Leconte, J., et al., *Nature*, 504, 268-271 (2013)
- 1469 Léger, A., et al., *Icarus*, 169, 499 (2004)
- 1470 Léger, A., et al., *A&A*, 506, 287-302 (2009)
- 1471 Lehmer, O. R., and Catling, D. C., *ApJ*, 845, 2 (2017)
- 1472 Lenton, T. M., and Watson, A. J., *Global Biogeochem. Cyc.*, 14, 249-268 (2000)
- 1473 Lewis, N. T., et al., *ApJ*, 854, 2 (2018)
- 1474 Li, Z.-X. A, and Lee, C.-T. A, *Earth Plan. Sci. Lett.*, 228, 483-493 (2014)
- 1475 Lin et al., *MNRAS*, 4890, 4338-4354 (2018)
- 1476 Lingam, M., and Loeb, A., *Int. J. Astrobiol.*, 1-10, doi:10.1017/S1473550419000247 (2018)
- 1477 Loftus, K., et al., *ApJ*, 887, 2 (2019)
- 1478 Lopez, E. D., and Rice, K., *MNRAS*, 479, 5303-5311 (2018)
- 1479 López-Morales, M., et al., *ApJ*, 158, 24 (2019)
- 1480 Lora, J. M., et al., *Icarus*, 250, 516-528 (2015)
- 1481 Lorenz, R. D., et al., *Geophys. Res. Lett.*, 24, 2905-2908 (1997)
- 1482 Luger, R., and Barnes, R., *Astrobiol.*, 15, 119-143 (2015)
- 1483 Lundkvist, M. S., et al., *Nature Comm.*, 7, 11201 (2016)
- 1484 Lunine, J. I., et al., *PSS*, 46, 1099-1107 (1998)
- 1485 Lupu, R. E., et al., *ApJ*, 670, 1473-1484, (2007)
- 1486 Lupu, R. E., et al., *ApJ*, 784, 27, 1-19 (2014)
- 1487 Madden, J., and Kaltenecker, L., *MNRAS*, (2020, accepted)
- 1488 Madhusudhan, N., *Ann. Rev. Astron. Astrophys.*, 57, 617-663 (2019)
- 1489 Madhusudhan, N., Agúndez, M., Moses, J. I., et al., *Space Sci. Rev.* 205, 285–348 (2016)
- 1490 Maeder, A., *Phys. Form. Evol. Rot. Stars*, 685-717 (2009)
- 1491 Mahapatra, G., et al., *MNRAS*, 472, 447-464 (2017)
- 1492 Mahieux, A., et al., *PSS*, 113-114, 193-204 (2015)
- 1493 Maldonado, J., et al., *A&A*, 612, A93 (2018)
- 1494 Mansfield, M., et al., *ApJL*, 868, 2 (2018)
- 1495 Marcq, E., et al., *JGR-E*, 10.1002/2016JE005224, 1539-1553 (2017)
- 1496 Markiewicz, W. J., et al., *Icarus*, 234, 200-203 (2015)
- 1497 Marty, B., *Nature*, 377, 326-329 (1995)
- 1498 Marty, B., *Earth Plan. Sci. Lett.*, 313, 56-66 (2012)
- 1499 Massol, H., et al., *Spa. Sci. Rev.*, 205, 153-211 (2016)
- 1500 Mazeh, T., et al., *A&A*, 589, A75 (2016)
- 1501 McKay, C. P., et al., *Science*, 253, 1118-1121 (1991)
- 1502 Martin, R. G., and Livio, M., *ApJ*, 822, 1-9 (2016)
- 1503 Mastrogiuseppe, M., et al., *Geophys. Res. Lett.*, 41, 1432-1437 (2014)
- 1504 Matrà, L. et al., *ApJ*, 859, 72 (2018)
- 1505 Matta, M., et al., *Icarus*, 204, 409-417 (2009)
- 1506 Maurice, M., et al., *J. Geophys. Res.*, 122, 577-598 (2017)

- 1507 Meadows, V., et al., *Astrobiol.*, 18, 630-682 (2018)
- 1508 Merkel, A. W., et al., *Icarus*, 281, 46-54 (2017)
- 1509 Miguel, Y., *MNRAS*, 482, 2893-2901, (2019)
- 1510 Mikhail, S., et al., *Geochim. Cosmochim. Acta*, 209, 149-160 (2017)
- 1511 Miyakawa, S., et al., *PNAS*, 99, 14,628-14,631 (2002)
- 1512 Modirrousta-Galian, D., et al., *ApJ*, 888, 1-87 (2020)
- 1513 Mojzsis, S. J., et al., *Nature*, 409, 178-181 (2001)
- 1514 Mollière et al., *A&A*, 600, A10 (2018)
- 1515 Morbidelli, A., and Raymond, S., *J. Geophys. Res.*, 121, 1962-1980 (2016)
- 1516 Mordasini, C., *A&A*, accepted (2020)
- 1517 Moreno, R. et al., *A&A* 608 L5 1-4 (2017)
- 1518 Morley, C. V., et al., *ApJ*, 815, 2 (2015)
- 1519 Moses, J. I., et al., 156, 76-106, *Icarus* (2002)
- 1520 Moses, J. I., et al., *Icarus*, 777, 34 (2013)
- 1521 Moses, J. I., et al., *Icarus*, 307, 124-145 (2019)
- 1522 Mousis, O., et al., 155, 12-40 (2018)
- 1523 Nachon, M., et al., *Icarus*, 281, 121-136 (2017)
- 1524 Nakajima, S., et al., *JAS*, 49, 2256-2266 (1992)
- 1525 Namouni, F., and Morais, M. H. M., *MNRAS*, 494, 2191-2199 (2020)
- 1526 Nettelmann, N., et al., *Icarus* 275, 107-116 (2015)
- 1527 De Niem, D., et al., *Icarus*, 221, 495-507 (2012)
- 1528 Niddever, D. L., et al., *ApJ*, 796, 1 (2014)
- 1529 Nikolaou, A., et al., *ApJ*, 875, 11, 1-24 (2019)
- 1530 Noack, L., et al., *Phys. Earth Plan. Int.*, 269, 40-57 (2017)
- 1531 Novelli, P. C., et al., *Science*, 263, 1587-1590 (1994)
- 1532 Nuecker, M. C., et al., *J. Ast. Tel. Inst. Sys.*, 2, 011001 (2016)
- 1533 Odert, P., et al., *Icarus*, 307, 327-346 (2018)
- 1534 Ohtani, E., *Nat. Spa. Rev.*, 7, 224-231 (2020)
- 1535 Oklopčić, A., et al., *ApJ*, 832, 30, 1-17 (2016)
- 1536 Olson, P., and Sharp, Z. D., *Earth Plan. Sci. Lett.*, 498, 418-426 (2018)
- 1537 Orton, G. S., et al., *Icarus*, 243, 494-513 (2014)
- 1538 Owen, J. E., and Mohanty, S., *MNRAS*, 459, 4088-4108 (2016)
- 1539 Owen, J. E., and Wu, Y., *ApJ*, 847, 1 (2017)
- 1540 Owen, J. E., *Ann. Rev. Earth Plan. Sci.*, 47, 67-90 (2019)
- 1541 Oza, A. V., et al., *ApJ*, 885, 168, 1-19 (2019)
- 1542 Pahlevan, K., et al., *Earth Plan. Sci. Lett.*, 301, 433-443 (2011)
- 1543 Von Paris, P., et al., *PSS*, 82-83, 149-154 (2013)
- 1544 Parmentier, V., et al., *ApJ*, 828, 1 (2016)
- 1545 Petsch, S. T., "The Global Oxygen Cycle" (2003)
- 1546 Pinilla, P., et al., *ApJ*, 845, 1 (2017)
- 1547 Pluriel, W., et al., *Icarus*, 317, 583-590 (2019)
- 1548 Poirier, J.-P., *Phys. Earth Plan. Int.*, 85, 319-337 (1994)
- 1549 Potter, A. E., and Killen, R. M., *Icarus*, 194, 1-12 (2008)
- 1550 Powell, D., et al., *ApJ*, 860, 1 (2018)
- 1551 Raines, J. M. et al., *J. Geophys. Res. Spa. Phys.*, 118, 1604-1619 (2014)
- 1552 Ramirez, R., et al., *Nat. Geosci.*, 7, 59-62 (2014)
- 1553 Randal Gladstone, G., et al., *Science*, 351, 6297 (2016)
- 1554 Raymond, S. N., and Cossou, C., *MNRASL*, 440, L11-L15, (2014)
- 1555 Ribas, I., et al., *ApJ*, 622, 680 (2005)
- 1556 Ridden-Harper, A. R., et al., *A&A*, 593, A129 (2016)
- 1557 Rimmer, P. B., et al., *Geochem. Perspec. Lett.*, 9,38-42 (2019)
- 1558 Rivoldini, A., et al., *Icarus*, 201, 12-30 (2009)
- 1559 Robinson, T. D., et al., *ApJ*, 787, 2 (2014)
- 1560 Rodler, F., and López-Morales, M., *ApJ* 781 54, 1-12 (2014)
- 1561 Rogers, T., *Nature Astron.*, 1, 0131, (2017)
- 1562 Rouan, D., et al. *ApJL*, 741, 2 (2011)
- 1563 Salvador, A., et al., *J. Geophys. Res.*, E122, 1458-1486 (2017)
- 1564 Samuel, B., et al., *A&A*, 563, A103 (2014)

- 1565 Schaefer, L., and Fegley, B., *APJL*, 703, 2 (2009)
- 1566 Schaefer, L., and Fegley, B., *Icarus*, 208, 438-448 (2010)
- 1567 Scheucher, M., et al., *ApJ*, 863, 6 (2018)
- 1568 Schmidt, J. A., et al., *PNAS*, 110, 17,691-17,696 (2013)
- 1569 Schmude R., in "Uranus, Neptune and Pluto and how to observe them", Springer (2008)
- 1570 Schubert, G., and Spohn, T., *J. Geophys. Res.*, 10.1029/JB095iB09p14095 (1990)
- 1571 Schwieterman, E., et al., *ApJ*, 810, 57, 1-15 (2015)
- 1572 Schwieterman, E., et al., *ApJL*, 821, 2 (2016)
- 1573 Selsis, F., Earth-like planets and moons, *Proc. 38th ESLAB symp.*, ISBN 92-9092-824-7, 251 - 258 (2002) Selsis, F., et al., *A&A*, 388, 985-1003 (2002)
- 1574 et al., *A&A*, 388, 985-1003 (2002)
- 1575 Sharp, Z. D., *Chem. Geol.*, 448, 137-150 (2017)
- 1576 Sheng, J.-X., et al., *J. Geophys. Res.*, 10.1002/2014JD021985, 1-21 (2015)
- 1577 Shizgal, B. D., and Arkos, G. G., *Rev. Geophys.*, 34, 4 (1996)
- 1578 Smith, G. P., and Nash, D., *Icarus*, 182, 181-201 (2006)
- 1579 Som, S. M., et al., *Nature*, 484, 359-362 (2012)
- 1580 Som, S. M., et al., *Nature, Geo.* 9, 448-451 (2016)
- 1581 Spake, J. J., et al., *Nature*, 68, 557, 68-70 (2018)
- 1582 Spohn, T. (ed.), *Planetary Evolution and Life Special Issue, PSS*, 1-268 (2014)
- 1583 Stern, S. A., et al., *Rev. Geophys.*, 37, 453-491 (1999)
- 1584 Stock, J. W., et al., *Icarus*, 291, 192-202 (2017)
- 1585 Sulis, S., et al., *A&A*, 631, A129 (2019)
- 1586 Stamenkovic, V., and Breuer, D., *Icarus*, 234, 174-193 (2014)
- 1587 Stüeken, E. E., et al., *Astrobiol.*, 16, 949-963 (2016)
- 1588 Svedhem, H., et al., *Nature*, 450, 629-632 (2007)
- 1589 Tabataba-Vakili, F., et al., *A&A*, 585, A96 (2016)
- 1590 Tambura, P., et al., *AJ*, 155, 5 (2018)
- 1591 Taylor, F. W., *Met. Appl.*, 17, 393-403 (2010)
- 1592 Taylor, S. R., and McLennan, S. M., *Rev. Geophys.*, 33, 241-265 (1985)
- 1593 Tian, F., and Ida, S., *Nat. Geosci.*, 8, 177-180 (2015)
- 1594 Tian, F., et al., *Earth Plan. Sci. Lett.*, 295, 412-418 (2009)
- 1595 Tian, F., et al., *Earth Plan. Sci. Lett.*, 379, 104-107 (2013)
- 1596 Tian, F., *Earth Plan. Sci.*, 385, 22-27 (2014)
- 1597 Tian, F., *Earth Plan. Sci.*, 43, 459-476 (2015a)
- 1598 Tian, F., *Earth Plan. Sci Lett.*, 432, 126-132 (2015b)
- 1599 Tian, F., et al., *Spa. Sci. Rev.*, 214, 65 (2018)
- 1600 Thomas, S. W., and Madhusudhan, N., *MNRAS*, 1330-1344 (2016)
- 1601 Tinetti, G., et al., *Nature*, 448, 169 (2007)
- 1602 Tinetti, G., et al., Chapter 16, in "Future observations of exoatmospheres from space" (ed. Forget, F., et al.), *Spa. Sci. Rev.* (in preparation) (2020)
- 1603 *Sci. Rev.* (in preparation) (2020)
- 1604 Tinetti, G., et al., *Exp. Astron.*, 46, 135-209 (2018)
- 1605 Tobie, G., et al., *Icarus*, 175, 496-502 (2005)
- 1606 Tobie, G., et al., *Nature*, 440, 61-64 (2006)
- 1607 Trail, D., et al., *Nature*, 480, 79-82 (2011)
- 1608 Tripathi, A., et al., *ApJ*, 808, 2 (2015)
- 1609 Tsiaris, A., et al., *ApJ*, 820, 1-13 (2016)
- 1610 Tucker, J. M., and Mukhopadhyay, S., *Earth Plan. Sci. Lett.*, 393, 254-265 (2014)
- 1611 Turbet, M., et al., *A&A*, 612, A86 (2018)
- 1612 Turbet, M., et al., *A&A*, 628, A12 (2019)
- 1613 Turbet, M., et al., *A&A*, 1-11 (2020, accepted)
- 1614 Vázquez-Semadeni, E., et al., *ApJ*, 643, 245-259 (2006)
- 1615 Venot, O., et al., *A&A*, 562, A51 (2014)
- 1616 Venturini, J., and Helled, R., *ApJ*, 848, 2 (2017)
- 1617 Vidotto, A. A., and Bourrier, V., *MNRAS*, 470., 4026-4033 (2017)
- 1618 Wakeford, H. R., et al., *MNRAS*, 464, 4247-4254 (2016)
- 1619 Walker, J. C. G., et al., *Geophys. Res.*, 86, C10, 9776-9782 (1981)
- 1620 Wang, X.-D, et al., *Nature Chem.*, 8, 258-263 (2016)
- 1621 Ward, L. M., et al., *Astrobiol.*, 19, 811-824 (2019)
- 1622 Warren, O. P., et al., *J. Geophys. Res.*, 124, 2793-2818 (2019)

- 1623 Way, M. J., et al., *GRL*, 43, 8367-8383 (2016)
- 1624 Weber, C., et al., *MNRAS*, 469, 3505-3517 (2017)
- 1625 Weiss, L. M., and Marcy, G. W., *ApJL*, 783, L6 (2014)
- 1626 Williams, D. M., and Pollard, D., *Int. J. Astrobiol.*, 1, 61-69 (2002)
- 1627 Wolf, E. T., and Toon, O. B., *Science*, 328, 1266-1268 (2010)
- 1628 Wong, M. H., et al., *Icarus*, 171, 153-170 (2004)
- 1629 Wong, M. L., et al., *Bull. Amer. Met. Soc.*, 51, 6 (2019)
- 1630 Wordsworth, R., and Pierrehumbert, R., *Science*, 339, 64-67 (2013)
- 1631 Wordsworth, R. D., *Earth Plan. Sci. Lett.*, 447, 103-111 (2016)
- 1632 Wordsworth, R. D., et al., *AJ*, 155, 1-25 (2018)
- 1633 Wu, J., et al., et al., *J. Geophys. Res. Plan.*, 10.1029/2018JE005698, 2691-2712 (2018)
- 1634 Yang, X., et al., *Earth Planet. Sci. Lett.*, 393, 201-219 (2014)
- 1635 Yang, J., et al., *AGU Fall Meeting, USA*, #P43E-2924 (2017)
- 1636 Yung, Y. L., and DeMore, W. B., "Photochemistry of planetary atmospheres" Oxford Uni. Press (1999)
- 1637 Zahnle, K., et al., *J. Geophys. Res.*, 113, 11004 (2008)
- 1638 Zahnle, K., et al., *ApJL*, 791, L20-L24 (2009)
- 1639 Zahnle, K., et al., *Cold Spr. Harb. Persp. Biol.*, 2:a004895 (2010)
- 1640 Zahnle, K., et al., *ApJ*, 824, 137, 1-17 (2016)
- 1641 Zarka, P., et al., *Res. Astron. Astrophys.*, 19, 2, 1-23 (2019)
- 1642 Zerkle, A. L., and Mikhail, S., *Geobiol.*, 15, 343-352 (2017)
- 1643 Zhu, X., et al., *Icarus*, 228, 301-314 (2014)
- 1644 Zilinskas, M., et al., *MNRAS*, 494, 1490-1506, (2020)
- 1645 Zolotov, M. Y., and Shock, E. L., *J. Geophys. Res.*, 109, E6, 1-16 (2004)